Class-I and Class-II fumarases are a paradigm of the recruitment of metabolites and metabolic enzymes for signalling of the DNA Damage Response during evolution.

Yardena Silas [1, 2], Esti Singer [1], Norbert Lehming [2] and Ophry Pines [1, 2]*

1. Department of Microbiology and Molecular Genetics, IMRIC, Faculty of Medicine, Hebrew University, Jerusalem, Israel
2. CREATE-NUS-HUJ Program and the Department of Microbiology and Immunology, Yong Loo Lin School of Medicine, National University of Singapore, Singapore, Singapore.

Yardena.silas@mail.huji.ac.il

esti.shai@mail.huji.ac.il

micln@nus.edu.sg

ophryp@ekmd.huji.ac.il

Abstract

Class-II fumarase (Fumarate Hydratase, FH) and its metabolic intermediates are essential components in the DNA damage response (DDR) in eukaryotic cells (human and yeast) and in the prokaryote *Bacillus subtilis*. Strikingly, here we show, in *Escherichia coli*, which harbors three fumarase genes; Class-I *fumA* and *fumB* and Class-II *fumC*, a variation of the distribution of function so far demonstrated (TCA cycle and DDR). Contrary to previous reports, *E. coli* Class-II fumarase participates naturally in respiration and the Class-I fumarases in the DDR. Contrary to other organisms, in *E. coli*, alpha-ketoglutarate (α-KG) is the organic acid that complements DNA damage sensitivity of *fum* null mutants. We show inhibition of the α-KG-dependent DNA damage repair enzyme, AlkB, by fumarate and succinate, and a global effect of fumarase absence on transcription. Together these results show an adaptable metabolic signalling of the DDR during evolution regardless of the enzyme Class preforming the DDR related function.

Introduction

Fumarase (fumarate hydratase, FH) is an enzyme that participates in the tricarboxylic acid (TCA) cycle, there, it catalyzes the reversible hydration of fumarate to L-malate (Woods, Schwartzbach, & Guest, 1988). In eukaryotes, in addition to its mitochondrial localization, a common theme conserved from yeast to humans is the existence of a cytosolic form of fumarase (Akiba, Hiraga, & Tuboi, 1984; Tuboi, Suzuki, Sato, & Yoshida, 1990). The dual distribution of fumarase between the mitochondria and the cytosol is a universal trait, but intriguingly, the mechanism by which dual distribution occurs does not appear to be conserved (Dik, Naamati, Asraf, Lehming, & Pines, 2016; Karniely, Regev-Rudzki, & Pines, 2006; Pracharoenwattana et al., 2010; Regev-Rudzki, Yogev, & Pines, 2008; Sass, Karniely, & Pines, 2003). We discovered that in eukaryotes the cytosolic form of this TCA enzyme was shown to have an unexpected function in the DNA damage response (DDR), and specifically, a role in recovery from DNA double strand breaks (DSBs) (Yogev et al., 2010). It appears that

metabolic signaling in these organisms is achieved via the fumarase organic acid substrate fumarate (Jiang et al., 2018; Leshets, Ramamurthy, Lisby, Lehming, & Pines, 2018). A recent study by Singer et al. (Singer, Silas, Ben-Yehuda, & Pines, 2017) shows that the Gram-positive *Bacillus subtilis* bacterial fumarase, has a role in the TCA cycle, yet also participates in the DDR. Fumarase dependent signaling of the DDR is achieved by its metabolic product, L-malate, which affects RecN (the first protein recruited to DNA damage sites) at the level of expression levels and localization. That study indicated that the dual function of this enzyme predated its dual distribution and, according to our model, was the driving force for the evolution of dual targeting in eukaryotes (Singer et al., 2017).

An intriguing variation to the themes above, is the fact that there are two distinct classes of fumarase. In the organisms mentioned above (*Sacchromyces cerevisiae*, human, *B. subtilis*) the fumarase that participates in both the TCA cycle and in DNA repair, belongs to the Class-II fumarase. In contrast, the Class-I fumarase, which bears no sequence or structural similarity to Class-II fumarases, is predominantly found in prokaryotes and in early evolutionary divergents in the eukaryotic kingdom (protozoa and invertebrates) (Woods et al., 1988). The model organism that we have employed in this study is the Gram-negative bacterium *E. coli* which harbors three fumarase genes; Class-I, *fumA* and *fumB* and Class-II, *fumC*. FumA and FumB are homologous proteins, sharing 90% amino acid sequence identity. Both FumA and FumB kinetic parameters are very similar with respect to the natural substrates L-malate and fumarate (van Vugt-Lussenburg, van der Weel, Hagen, & Hagedoorn, 2013). FumC is homologous to eukaryotic and *B. subtilis* fumarases, sharing 64% amino acid sequence identity with eukaryotic and *B. subtilis* fumarases.

Employing the *E. coli* model, we ask whether Class-I and/or Class-II fumarases are involved in the DDR and/or the TCA cycle and what is the distribution of functions between these two Classes of fumarases in this organism. Here we show that FumA and FumB are participants of the DDR in *E. coli*, while FumC naturally participates in respiration. FumA and FumB participation in the DDR is based on a fascinating interplay of TCA cycle Intermediates, alpha-ketoglutarate (α-KG), fumarate and succinate. In *E. coli* the absence of fumarase is shown to

affect the transcription of many genes following DNA damage induction, including many DNA repair genes. Specifically, we show that the target of alpha-ketoglutarate is the α-KG-dependent DNA repair enzyme AlkB demethylase which is required for successful repair of DNA damage and which is also modulated by fumarate and succinate.

Results

ΔfumA and *ΔfumB* but not *ΔfumC E. coli* strains, are sensitive to DNA damage induction.

In order to examine a possible role for *E. coli* fumarases in the DNA damage response, we induced DNA damage in *E. coli* strains lacking each of the fumarase genes, by exposing them to treatment with Ionizing radiation (IR, Fig. 1A) or methyl methanesulfonate (Fig. 1B, MMS, 0.35% [v/v] for 30 or 45 minutes). Figures 1A and 1B (compare rows 2 and 3 in each panel to row 1) demonstrate that compared to the control (WT), strains lacking *fumA* or *fumB* are very sensitive to DNA damage (IR or 0.35% [v/v] MMS for 45 minutes), while the strain lacking *fumC* seems unaffected by the DNA damage induction (row 4). These results suggest that FumA and FumB play a role in the DNA damage response, while FumC has no observable role in this process. While the levels of FumA exhibit a very insignificant change in protein levels upon treatment with MMS (Fig 1c top panel), the levels of FumC increase (Fig 1C second panel), thereby revealing a more complex picture of regulation. Intriguingly, the double mutant (Fig 1D, middle panel, *ΔfumAB,* Row 5) is resistant to DNA damage induction, either IR or MMS treatment and shows a phenotype resembling the WT strain (Row 1), when compared to single *fumA* and *fumB* deletion strains (*ΔfumA, ΔfumB,* rows 2 and 3) or a triple mutant lacking all three fumarase genes (*ΔfumACB,* row 6) which are sensitive to IR and MMS. One possible explanation for this phenomenon is that in the absence of FumA and FumB, FumC expression, which is much lower at basal levels (i.e. no MMS treatment) increases to undertake both roles of respiration and participation in the DDR (Fig 1E). Worth mentioning

here and referred to in the next section, is that complementation of the DNA damage sensitivity can be achieved by the genes in trans (Fig 3).

All three *E coli* fumarase genes can participate in the TCA cycle.

It is important to emphasize, with regard to respiration, that a functional TCA cycle including participation of fumarase is required (Figure 1D, right panel). Accordingly, we find growth of our strains (WT, *ΔfumA*, *ΔfumB, ΔfumC* and *ΔfumAB)* which harbour at least one functional fumarase gene, on minimal media with acetate as a sole carbon and energy source. In contrast the triple mutant (*ΔfumACB*), completely lacking fumarase, is unable to respire and therefore unable to grow on this media (Figure 1D, right panel row 6). The *ΔfumC* mutant shows an interesting respiration phenotype, although FumA and/or FumB seem to participate primarily in the DDR, it would seem that in the absence of FumC, these enzymes have the ability to participate in respiration, but likely play a less critical role in this function. Figure 1F shows the relative enzymatic activity of each of the mutant strains compared to the WT. These strains were assayed for fumarate production using L-malate as a substrate, testing its depletion at 250nm, there is an observable decrease in enzymatic activity in fumarase mutant strains when compared to the WT (*ΔfumA* 50%, *ΔfumB* 30%, *ΔfumC* 90%, *ΔfumAB* 50% and *ΔfumACB* with insignificant activity). After treatment with MMS, the WT exhibits a 40% reduction in enzymatic activity and the mutants also exhibit an additional reduction in enzymatic activity (e.g. *ΔfumA 10%, ΔfumB 15%, ΔfumAB 5%)* when compared to the same untreated strain. The sharp decrease of fumarase activity in ***ΔfumC*** indicates that FumC is responsible for most of the fumarase activity in *E. coli*. FumA and FumC protein levels of these strains under the same conditions are shown in figure S1A. These strains also show an expected decrease in FumC protein levels in the mutants compared to the WT strain, coupled with further reduction in FumC levels following MMS treatment (with the exception of the *ΔfumAB* strain as shown above). FumA levels in *ΔfumB* and *ΔfumC* strains resemble the FumA

levels observed in the WT strain before induction of DNA damage, but show more significant reduction in FumA levels compared to the WT strain following MMS treatment.

As controls for the above experiments, we show that over-expression of FumA, FumB or FumC from high copy number plasmids (pUC-18) in the triple fumarase mutant (*ΔfumACB*) brings about a partial complementation of DNA damage sensitivity while only FumC appears to fully complement respiration (Fig. S1B). The expression levels of each of these constructs is shown in Fig. S1C. Due to fact that these experiments are not under natural induction, but rather under over-expression conditions, FumC seems to have the same effect as FumA and FumB in regard to DNA damage induction. But in reference to the above experiment, it is also evident that under conditions of *fumA* and *fumB* absence, FumC, which is then overexpressed and takes over this role to participate in the DDR.

***E. coli* fumarases function in both the DDR and respiration in a yeast model system.**

In order to validate that indeed FumA and FumB participate in the DNA damage response and FumC participates in respiration, we employed, as in the past (Singer et al., 2017; Yogev et al., 2010), the yeast *Saccharomyces cerevisiae* as a model. We cloned each of these genes into yeast expression vectors and transformed them into two different yeast strains. The first yeast strain, Fum1M, harbors a chromosomal *fum1* deletion (*Δfum1*) and a *FUM1* open reading frame insertion in the mitochondrial DNA. This allows exclusive mitochondrial fumarase expression, lacking extra-mitochondrial (cytosolic/nuclear) fumarase (Yogev et al., 2010). This Fum1M strain which is sensitive to DNA damage was transformed with each of the fumarases separately (Fig. 2A) in order to test whether bacterial FumA and FumB are able to protect against DNA damage, a function of the cytosolic yeast fumarase. To this end, we induced DNA damage by IR as shown in Fig. 2A or hydroxyurea (HU, not shown). Compared to the WT and Fum1M strains (rows 1 and 2 respectively), *E. coli* FumA and FumB are able to protect yeast from DNA damage while FumC does not (rows 3, 4 and 5 respectively).

The second yeast strain completely lacks fumarase *(Δfum1*) and therefore lacks respiration ability. We transformed each of the fumarase genes separately (Fig. 2B) and growth was followed on synthetic complete (SC) medium supplemented with ethanol (as a sole carbon and energy source). Compared to the Δ*fum* strain that lacks respiration ability (Fig. 2B, compare row 2 to row 1), and to the Δ*fum* that harbors yeast Fum1 encoded from a plasmid (row 3), FumA and FumB are unable to complement respiration while FumC partially complements respiration (rows 4, 5 and 6 respectively). The expression levels of each of these constructs is similar relative to the loading control aconitase (Fig. 2C). As FumA and FumB harbour no structural similarity to the yeast fumarase, this result does not definitively mean that they do not participate in respiration, but that due to evolutionary structural incompatibility with other cellular machinery, these enzymes are not able to complement respiration in this higher organism.

Previous unpublished work from our lab (Burak MSc thesis, Pines lab), demonstrated that fusion of the fumC coding sequence to *Neurospora crassa* F_o-ATPase, Su9 mitochondrial targeting sequence, led to complete import and processing of *E. coli* FumC in mitochondria. Without this sequence, FumC is not in mitochondria, but can complement yeast *fum* null mutants in cell respiration due to transport of the organic acid substrates (fumarate and L-malate) in and out of the organelle. The complementation of DNA damage sensitivity by FumA and FumB indicates that these enzymes indeed participate in the DDR and this function is evolutionary conserved as seen before (Singer et al., 2017), while FumC participates in the TCA cycle and respiration in *S. cerevisiae*.

FumC is homologous to eukaryotic fumarase and to *B. subtilis* fumarase, and as referred to above, the cytosolic role of these fumarases is in the DDR. Intriguingly, in *E. coli* this role is carried out by FumA and FumB, although they have no sequence or structural similarity to the Class-II fumarases, besides their activity. To challenge this apparent distribution of functions between *E. coli* Class-I and Class-II fumarases and, in particular, the inability of FumC to function in the DDR, we asked whether this is due to a problem in the localization of FumC in the nucleus. As previous research shows that upon DNA damage induction there is migration

of fumarase to the nucleus, there it participates in various DNA damage repair pathways (Jiang et al., 2018; Yogev et al., 2010), the approach we took was to force the FumC protein into the yeast nucleus. We constructed a *fumC* ORF fused to a nuclear localization sequence (NLS). The modified protein was expressed in a yeast Fum1M strain and the respective strains were grown with or without HU (Fig 2D). We found that the modified FumC, containing an NLS was capable of complementing the Fum1M sensitivity to HU (Fig 2D, row 5). As controls we show that the original FumC, a FumC that harbors a nuclear export signal (NES) (row 4) or a FumC harboring a mutated NLS (mNLS, row 6) (Fig. 2D) do not complement Fum1M strain sensitivity to HU. The expression levels of each of these constructs is similar relative to the loading control aconitase (Fig. 2E). The NES sequence once fused to FumA (FumA-NES) or FumB (FumB-NES), render these enzymes completely incapable of protecting fum1M against DNA damage (Fig. S2A, S2B). Figure S2C depicts expression of these modified proteins.

FumA and FumB enzymatic activity is required for their DNA damage response function.

We have previously shown that the enzymatic activity of Class-II fumarases is required for their role in the DNA damage response (Singer et al., 2017; Yogev et al., 2010). In order to ask whether the same is true regarding Class-I enzymes, FumA and FumB, we first needed to obtain enzymatically compromised mutants of these proteins. For this, we designed substitution mutations based on the predicted structure of *E. coli* Class-I fumarases according to the solved crystal structure of Class-I FH of *Leishmania major* (LmFH). We focused on the most conserved amino acids within a pocket that is suggested to be important for its catalytic activity (Feliciano, Drennan, & Nonato, 2016). Figure 3A depicts a dimeric homology model of the proposed structure for either FumA or FumB proteins which share 90% amino acid identity, and it is believed that they possess the same structure. The residues shown in spherical mode represent the dimeric enzyme interface that together form a cavity that in LmFH leads to the active site. Figure 3B shows alignment of the proposed *E. coli* Class-I fumarase structure (green) with that of *L. major* (blue, red, orange and yellow). We cloned PCR products harboring

the point mutations into appropriate *E. coli* expression vectors. These plasmids were transformed into *E. coli* strains lacking each of the respective genes (Fig. 3C, 3D) and their expression was examined by Western blot (3E). Upon exposure to DNA damage (0.35% [v/v] MMS, 45 min), we observed an inability of the variant enzymes to protect against DNA damage in *E. coli* (Fig. 3C and 3D, compare rows 4 and 5 to row 3). The fumarase null mutant strain harboring these plasmids exhibits a highly significant reduction in enzymatic activity compared to wild-type FumA and FumB (Fig. 3F, 3G, compare bars 3 and 4 to bars 2). These results indicate that the enzymatic activity of FumA and FumB is crucial for their DDR related functions of fumarase in *E. coli*.

Alpha-Ketoglutarate complements DNA damage sensitivity of *E. coli fum* null mutants. In *S. cerevisiae* and human cells, the lack of extra mitochondrial fumarase and resulting sensitivity to DNA damage, can be complemented by externally added fumarate (fumaric acid, in the form of an ester, mono-ethyl fumarate, which is cleaved in the cells to form the free acid) (Jiang et al., 2018; Yogev et al., 2010). In *B. subtilis* the sensitivity of a fumarase null mutant to DNA damage, can be complemented by L-malate (Singer et al., 2017). To examine if fumarase associated metabolites (substrates or products) complement the lack of fumarase in the DDR of *E. coli*, bacteria were grown in the presence of 25mM TCA cycle organic acids, added to the medium. Intriguingly, as shown in Figure 4, *E. coli* strains deleted for the *fumA*, *fumB* and all three *fum* genes are protected from MMS induced DNA damage (0.35% [v/v] MMS, 45 min) by α-KG (bottom panel, compare rows 2, 3 and 6 to rows 1 and 4) and not by fumarate or L-malate (panels 5 and 6 respectively). This complementation can be achieved by concentrations as low as 1mM α-KG added to the growth medium (data not shown). Growth of these strains on LB metabolite plates, shows growth consistent with that of the controls (top panel). α-KG does not protect *E. coli* strains harboring deletions in other DNA damage response genes (Fig S3) or composite mutants of DDR genes and *fumA*/*fumB* from DNA damage induction, suggesting a direct relationship between fumarase and α-KG within the DNA damage response of *E. coli*.

To investigate this relationship, we decided to study the α-KG effect on two different levels; the first being to investigate a global impact of α-KG on transcription and induction of DNA repair pathways in *E. coli*. The second was to investigate a direct impact on the activity of DNA repair related proteins.

Absence of *E. coli* fumarases affect the transcript levels of many genes including adaptive and SOS response genes.

In *E. coli*, there are multiple DNA repair pathways, including; LexA-dependent SOS response triggering Homologous Recombination Repair (HRR), LexA-independent DNA damage responses and the Adaptive Response. MMS as well as UV-irradiation and other chemicals are capable of inducing the SOS response. The SOS response triggers HRR in *E. coli*, which proceeds via two genetic pathways, RecFOR and RecBCD. The RecBCD pathway is essential for the repair of DSBs and the RecFOR pathway for GAP repair (Baharoglu & Mazel, 2014). The Adaptive Response involves the transcriptional induction of several genes in response to alkylation damage to the DNA caused by MMS treatment, among them *ada* (transcriptional regulator of the adaptive response), *alkA*, *alkB* and *aidB* (Errol et al., 2006; Kreuzer, 2013). Given that the *fumA* and *fumB* single null and the *fumACB* triple null mutants are sensitive to DNA damage, compared to the wild type, and the apparent complementation of the DNA damage sensitivity phenotype by α-KG, we decided to study the transcriptional profiles of *fum* null mutants vs the WT strain via RNA-seq. The objective of the RNA-seq analysis was to find differentially expressed genes (DEGs, up or down regulated) in the WT strain in response to MMS treatment (0.35% [v/v],30 min), and more importantly in response to MMS+α-KG (0.35% [v/v], 30 min +25mM α-KG when indicated), compared to the mutant strains. This analysis was conducted in an effort to identify α-KG dependent enzymatic or regulatory components involved in the DNA damage sensitive phenotype. Total RNA was extracted from three independent replicates, and RNA-seq analysis was performed (see materials and methods). To determine statistically significantly up or down regulated genes, a criterion of log ≥2.0-fold change or greater was used. The results are presented as Venn diagrams in figure 5A, 5B,

S4A and S4B and Column diagram in Fig 5C. The corresponding raw data lists of all DEGs are presented in supplementary table 1.

Figure 5A, 5B and S4A depicts changes in gene expression between the WT strain and the *fum* null mutant strains, following treatment with MMS or MMS + α-KG. Treatment with MMS coupled with α-KG does not significantly change the total number of genes with altered expression (S4B). All transcripts, shared and exclusive to each strain were analysed using the web Gene Ontology Resource tool (Ashburner et al., 2000; "The Gene Ontology Resource: 20 years and still GOing strong," 2019).

Of the upregulated genes, common to all tested strains (WT, *ΔfumA, ΔfumB* and *ΔfumACB*) we detect an upregulation of DNA repair and DNA recombination genes (SOS response genes, HRR genes, adaptive response genes) and other stress response genes (oxidative stress response genes, various chaperones and others). Importantly, this is regardless of treatment with α-KG in addition to MMS or not. Of the downregulated genes, common to all tested strains (WT, *ΔfumA, ΔfumB* and *ΔfumACB*) we detect, downregulation of genes regulating cell growth, genes regulating cellular division and others.

Most important, analysing DEGs altered exclusively in the WT strain or exclusively in either *fum* mutant strain (supplementary table 2), yielded no candidate genes that may explain the DNA damage sensitivity of *ΔfumA, ΔfumB* and *ΔfumACB* strains, as all DNA repair systems seem to be induced in all strains. For this reason, we decided to look specifically at the induction levels (fold change in expression) of DNA repair genes and see if there is any direct effect resulting from the absence of fumarase. Examples of SOS response genes (*lexA*, *recA*, *umuD*, *polB*, *dinB*, *dinI* and *ssb*), Adaptive response genes (*alkA* and *alkB*) and genes controlling cell division (*sulA*, *ftsZ*, *minC* and *minD*) are presented in Figure S4C-P. As mentioned above, we find induction of the SOS and the adaptive response genes in the presence of MMS or MMS+ α-KG in all strains coupled with the decrease in cell division genes, demonstrating a need for inhibition of the cell cycle for the repair of the damaged DNA. For *lexA*, *recA*, *umuD*, *alkA*, *alkB*, *ssb* there is a significantly higher expression level in the WT

strain compared to the *fum* null mutant strains. It is important to emphasise that α-KG has no additive effect to treatment with MMS alone on the expression levels of these genes.

In order to validate the reproducibility and accuracy of the RNA-seq analysis results, we determined the mRNA levels of four DDR and stress response genes by RT-qPCR; *recA, dinI*, *alkA* and *alkB*. All strains were grown as per the RNA-seq experiment in three independent replicates (0.35% [v/v] MMS, 30 min +25 mM α-KG when indicated). The results are consistent with those of the RNA-seq data (Fig S5A-D) primers used for this assay are presented in supplemental table 3.

Why do *E. coli fum* null mutants exhibit a lower expression of these various DDR genes or even a higher expression level of other genes? Whether this effect is mediated by fumarase metabolites, fumarate or malate, as seen in other systems remains to be studied (Kronenberg et al., 2019; Sciacovelli & Frezza, 2017; Sciacovelli et al., 2016). In this regard, we find insignificant differences in the levels of fumarate and α-KG in the extracts of wild type, *ΔfumA, ΔfumB* and *ΔfumC* cells, in the presence or absence of MMS by LC-MS (data not shown). Thus, the cellular levels do not appear to be at the root of this phenomenon.

Alpha-ketoglutarate enhances, whereas succinate and fumarate inhibit AlkB DNA damage repair activity.

Our most important conclusion from the previous section is that the candidate DNA damage signalling metabolite, α-KG, does not function at the level of transcription. Given these results, we chose to focus on DNA repair enzymes whose activity may be regulated by TCA cycle organic acids. We decided to focus on AlkB due to its known function in DNA damage repair and its interaction with α-KG. AlkB is a Fe-(II)/α-KG-dependent dioxygenase in *E. coli* which catalyses the direct reversal of alkylation damage to DNA, primarily 1-methyladenine (1mA) and 3-methylcytosine (3mC) lesions. A hallmark of AlkB-mediated oxidative demethylation is that the oxidized methyl group is removed as formaldehyde (Falnes, Klungland, & Alseth, 2007). Previously published research in the bacterium *B. subtilis* showed that in fumarase null mutants, there is an accumulation of succinate and fumarate (Singer et al., 2017). In

eukaryotes, fumarate and succinate have been shown to inhibit human α-KG-dependent histone and DNA demethylases and in yeast, fumarate inhibits the sensitivity of components of the homologous recombination repair system to DNA damage induction (Jiang et al., 2018; Leshets et al., 2018; Xiao et al., 2012). The inhibition of histone and DNA α-KG-dependent demethylases by fumarate and succinate was established as competitive, based on their structural similarity to α-KG (Xiao et al., 2012).

To test whether fumarate and succinate inhibit AlkB demethylase activity in *E. coli*, we employed two previously published protocols (Shivange, Kodipelli, & Anindya, 2014; Shivange, Monisha, Nigam, Kodipelli, & Anindya, 2016) for in vitro measurement of DNA damage repair by AlkB in the presence and absence of succinate, fumarate and malate. Such an effect, if found could explain the increase in sensitivity of *fum* null mutants to MMS generated DNA damage.

The first approach was direct fluorescence-based formaldehyde detection using acetoacetanilide and ammonium acetate, which together form an enamine-type intermediate. This intermediate undergoes cyclodehydration to generate highly fluorescent dihydropyridine derivative, having maximum excitation at 365 nm and maximum emission at 465 nm (Shivange et al., 2016). A 70bp oligonucleotide (see materials and methods) was treated with MMS to allow methylation, and was directly incubated with purified AlkB to facilitate DNA repair. DNA repair was measured by release of formaldehyde (RFU [HCHO concentration]). While α-KG is required for the full activity of AlkB in vitro (Figure 6A, bar 1, 200μM of α-KG), succinate and fumarate competitively inhibit E. coli AlkB demethylase activity in a dose dependent manner (compare bars 2-4, 5-7 to bar 1) (200μM of succinate and fumarate with increasing amounts of α-KG). Malate appears to have an insignificant, non-dose dependent, effect on AlkB demethylase activity (bars 8-10) (200μM of malate with increasing amounts of α-KG).

The second approach, employs a restriction enzyme-based demethylation assay (Shivange et al., 2014). The same substrate (70bp oligonucleotide substrate that contains the MboI restriction enzyme recognition site in the middle of the sequence) was treated with MMS to

allow methylation, and was directly incubated with purified AlkB to facilitate DNA repair. By digestion with the dam methylation sensitive enzyme MboI, successful repair of methylated oligonucleotide (complete demethylation by AlkB) yields a 35bp product (Fig 6B, compare lane 4 to lane 3 [methylated dsDNA [me-dsDNA] undigested by MboI] and lane 2 [control un-methylated dsDNA digested by MboI]). Shown in Figure 6B, is the inhibition of AlkB demethylase activity which can be detected by the non-apparent 35bp fragment. Succinate and fumarate inhibit AlkB in a dose dependent manner (compare lanes 5-8 [containing 200 μM succinic acid and increasing concentrations of α-KG] and lanes 9-12 [200 μM fumaric acid and increasing concentrations of α-KG] to lane 4 [containing 200 μM α-KG]). Malate appears to have an insignificant effect on AlkB demethylase activity (lanes 13-16). Together, these results demonstrate, for the first time, *E. coli* AlkB inhibition by fumarate and succinate.

In order to validate these results in vivo, an AlkB inhibition experiment with high molar concentrations (25mM) of fumarate and succinate was carried out. For this purpose, we induced DNA damage (using 0.35% [v/v] MMS, 45 min) in an *E. coli* strain lacking *alkB* (*ΔalkB*), and in a *ΔalkB* strain, overexpressing AlkB from a plasmid. Figure 6C shows that *ΔalkB* is extremely sensitive to MMS generated DNA damage, and overexpression of AlkB completely compensates for this DNA damage sensitivity phenotype (panel 2, compare row 3 to row 2). Fumarate and succinate exhibit a strong inhibition of AlkB ability to repair damaged DNA (compare top row, panels 4 and 5 to panels 2 and 3). Addition of as low as 1 mM of α-KG complements AlkB activity in vivo (compare bottom row, panels 2 and 3 to top row panels 4 and 5). These results are consistent with the previously shown in vitro experiments above, in which fumarate and succinate strongly inhibit AlkB DNA repair activity with malate having no effect on the AlkB DNA repair function. These results are summarized in a model in which the inhibition of α-KG-dependent-AlkB by accumulation in vivo of fumarate and succinate leads to the sensitivity of *ΔfumA, ΔfumB* and *ΔfumACB* to DNA damage (Fig. 6D).

Discussion

Recent discoveries identify the recruitment of metabolic intermediates and their associated pathways in the signalling of crucial cellular functions. The best example is the enzyme fumarase (fumarate hydratase) which belongs to Class-II (FumC-like fumarases). This TCA cycle enzyme has been shown to be involved in the DNA damage response in yeast and human, and more recently in the Gram-positive bacterium *B. subtilis* (Jiang et al., 2018; Johnson, Costa, Ferguson, & Frezza, 2018; Leshets et al., 2018; Singer et al., 2017). In human and yeast, fumarate (fumaric acid) is the signalling molecule targeting histone demethylases and a HRR resection enzyme respectively (Jiang et al., 2018; Leshets et al., 2018). In *B. subtilis* L-malate is the signalling molecule, modulating RecN (the first enzyme recruited to DNA damage sites) expression levels and cellular localization (Singer et al., 2017). In this study we show an amazing variation on the above themes by studying *E. coli*, which harbors the two Classes of fumarases, Class-I *fumA* and *fumB* and Class-II *fumC*. At first glance, contrary to previous work on Class-II fumarases, *E. coli* FumC does not have a natural role in the DDR, while FumA and FumB, harboring no structural or sequence similarity to the Class-II fumarases, are participants in the DDR in this Gram-negative bacterium. In this regard, not only do FumA and FumB participate in the DDR in *E. coli*, they can substitute for yeast fumarase in a Fum1M DNA damage sensitive model strain (Singer et al., 2017; Yogev et al., 2010). This shows that Class-I fumarases, FumA/FumB, that are non-homologous to the yeast Class-II fumarase, can function in the DDR, indicating that not the enzyme is needed for this DDR related function, but rather its enzymatic activity and related metabolites. As we have demonstrated for Class-II FH in human cell lines, yeast and *B. subtilis*, FumA and FumB enzymatic activity is crucial for their DNA damage protective function. This is supported in this study by the fact that enzymatically compromised variants of the Class-I fumarase do not signal the DDR. Our results indicate that it is only the level of fumarase activity that is important, since if over-expressed all three *fum* genes can function in the DDR in *E. coli*.

Most interesting is, that neither fumarate nor malate added to the growth medium are capable of complementing the DNA damage sensitive phenotype of *fum* null mutants as demonstrated for the previously studied organisms. α-KG, a TCA cycle intermediate with no direct interaction

with fumarase appears to be the signalling metabolite. Moreover, this α-KG mediated protective effect seems to be exclusive to *fum* null mutants, as the sensitivity phenotype of other *E. coli* null mutants in DNA damage repair genes, is not alleviated by the addition of α-KG to the growth medium. On the one hand, fumarase absence specifically affects the activity of the DNA repair enzyme AlkB, and leads to a reduced transcriptional induction of DNA damage repair components, on the other.

The absence of fumarase is shown here to affect AlkB, a Fe-(II)/α-KG-dependent dioxygenase via its precursor metabolites succinate and fumarate. Fe-(II)/α-KG-dependent dioxygenases are present in all living organisms and catalyse hydroxylation reactions on a diverse set of substrates, including proteins, alkylated DNA/RNA, lipids and others (Hausinger, 2004; Loenarz & Schofield, 2008). Fumarate and its precursor succinate have been shown to inhibit a variety of Fe-(II)/α-KG-dependent dioxygenases, and this inhibition was shown to antagonize α-KG-dependent processes and negatively regulate Fe-(II)/α-KG-dependent dioxygenases such as prolyl hydroxylases (PHDs), histone lysine demethylases (KDMs), collagen prolyl-4-hydroxylases, and the TET (ten-eleven translocation) family of 5-methlycytosine (5mC) hydroxylases (Gottlieb & Tomlinson, 2005; Jiang et al., 2018; Johnson et al., 2018; Pollard et al., 2005; Selak et al., 2005; Tahiliani et al., 2009; Xiao et al., 2012). We find, in agreement with the above observations, that AlkB enzymatic activity is inhibited by the presence of high concentrations of fumarate and succinate both in vitro and in vivo, indicating that AlkB inhibition has a specific consequence in vivo, leading to the sensitivity of *ΔfumA, ΔfumB* and *ΔfumACB* to DNA damage.

The above findings suggest that the recruitment of metabolic intermediates and their associated pathways in signalling during evolution, was adaptable. In an ongoing study we are examining the distribution of Class-I and Class-II fumarases through the different domains of life. Class-I and Class-II can be found in prokaryotes and eukaryotes as sole fumarase representatives; e.g. mammals harbour only Class-II while many protozoa contain only Class-I fumarases. Some organisms, such as *E. coli*, harbour both Classes and, in fact, very few

can be found that lack both Classes of fumarases. At this stage it is difficult for us to hypothesise why a certain metabolite, Class of enzyme, or pathway was chosen to signal the DDR, but this study gives us a new perception on how metabolites, metabolic enzymes and pathways could have been recruited during evolution of metabolite signalling.

There are many unanswered questions regarding the fumarases in *E. coli*, for example does subcellular localization of the fumarases or their metabolites play a role in their DDR function? Using specific Class-I and Class-II antibodies we detect that the enzymes do not co-localize with the nucleoid but rather localize to the cell poles regardless of treatment with MMS (not shown). What governs the levels of α-KG and other metabolites at sites of DNA damage? And how exactly does fumarate exert its effect on transcription? Further studies are needed to address these complex questions and systems.

Materials and methods

1. Bacterial Strains and Growth Conditions

Bacterial strains were provided by the Coli Genetic Stock Center and are listed in supplementary table 4. Additional strains were constructed using the lambda red system (Datsenko & Wanner, 2000), plasmids were constructed using standard methods, plasmids and primers are listed in supplementary table 5. Bacteria were grown in Luria-Bertani (LB) broth to early to mid-exponential phase (OD_{600nm}=0.35), supplemented, when needed, with ampicillin (Amp, 100 g/ml) or 25 mM metabolites (α-KG, succinate, fumarate, malate [Sigma Aldrich]). MMS was added to a final concentration of 0.35% [v/v]. When indicated 0.5 mM of IPTG (isopropyl-D-thiogalactopyranoside, Sigma) was added. For agar plates, 2% agar was added.

2. Yeast Strains and Growth Conditions

S. cerevisiae strains used in this research are listed in supplementary table 6. *S. cerevisiae* strains used were grown on synthetic complete (SC) medium containing 0.67% (wt/vol) yeast nitrogen base +2% glucose (SC-Dex) or 2% galactose (SC-Gal) (wt/vol), supplemented with

appropriate amino acids. For agar plates, 2% agar was added. HU was added to SC medium (supplemented with glucose) to a final concentration of 200 mM. The cells were grown overnight at 30ºC in SC-Dex, washed in sterile double distilled water and transferred to SC-Gal for induction of genes under GAL promoter.

3. Construction of mutants- Gene knockout using λ red system (pKD46)

3.1 Gene Disruption

Δ*fumAB*, Δ*fumACB* strains (and other composite mutants in this study) were constructed by the following: Gene disruption as previously described (Datsenko & Wanner, 2000). Essentially, Δ*fumB* and BW25113 Transformants carrying λ red plasmid were grown in 5-ml LB cultures with ampicillin and L-arabinose at 30°C to an OD_{600} of 0.6. The cells were made electrocompetent by concentrating 100-fold and washing three times with ice-cold sterile DDW. Electroporation was done by using a Cell-Porator with a voltage booster and 0.2-cm chambers according to the manufacturer's instructions (BIO-RAD). By using 100 µl of suspended cells and 100 ng of PCR product (for Δ*fumAB* strain cat cassette with flanking upstream and downstream sequences of *fumA*, and for Δ*fumAC* strain cat cassette (Chloramphenicol, Cm) with flanking upstream of *fumA* and downstream of *fumC*), the cells were added to 1-ml LB, incubated 3 hours at 37°C, and then spread onto agar supplemented with Cm/Kan to select CmR/KanR transformants. After primary selection, mutants were colony purified twice selectively at 37°C and then tested for loss of the parental gene by PCR.

Following verification of *fumAC* knock out and cassette insertion, a second Knock out was carried out with Kan (Kanamycin) cassette with flanking upstream and downstream of *fumB* [two step Gene knockout]).

3.2. PCR verification of gene disruption

Two PCR reactions were used to show that the mutants have the correct structure. A freshly isolated colony was used in separate PCRs following a 5-min pre-incubation ''hot start,'' at 95°C. One reaction was done by using nearby locus-specific primers (150bp upstream of *fumA* or *fumB*) with the respective common test primer (c1 and k2) to verify gain of the new mutant specific fragment (antibiotic resistance), and a second reaction was carried out with the

flanking locus-specific primers to verify simultaneous loss of the parental (non-mutant) fragment. Control colonies were always tested side-by-side.

4. Prediction of FumA and FumB structure

Prediction of FumA and FumB were as previously described (Ben-Menachem et al., 2018). Essentially, Homology models of the structure of *E. coli* FumA and FumB (based on the solved structures of 5L2R of *L. major*, (Feliciano et al., 2016)) were generated using I-TASSER (Yang et al., 2015). The models with the highest probability score among the provided models were selected for further investigation. Using PeptiMap (Bohnuud, Jones, Schueler-Furman, & Kozakov, 2017) for the identification of peptide binding sites and CONSURF (Ashkenazy et al., 2016) for conservation analysis of FumA and FumB amino acid sequence. Mutations were designed based on conserved amino acids within the peptide binding pockets detected. Figures of structures were generated using the PyMOL software (Schrödinger Inc).

4.1. Mutagenesis of suspected catalytic site

Three proposed amino acids suspected to be vital for the suspected catalytic site of FumA and FumB*;* Isoleucine 233, Threonine 236 and Tyrosine 481 were mutagenized by site directed mutagenesis with a KAPA HiFi HotStart PCR kit (KAPABIOSYSTEMS). Exchanging Tyrosine, at 481 with Aspartic acid (Y481D). We chose to combine I233 and T236 generating a double point mutation, exchanging Isoleucine at 233 for lysine, and exchanging Threonine at 236 with Isoleucine (I233K T236I). All mutated genes were cloned into Puc18 cloning vector and transformed into bacterial strains Δ*fumA*, Δ*fumB* and yeast strains Fum1M and Δ*fum1*.

5. FumA/FumB activity assay

Fumarase activity of FumA and FumB were assayed as previously described (van Vugt-Lussenburg et al., 2013). Essentially, fumarase enzymatic activity was measured by monitoring malate depletion at 250 nm spectrophotometrically in quartz cuvettes (Fumarase activity at 250 nm with L-malic acid as the substrate). Assays were performed in assay buffer (100 mM Hepes buffer pH 8 with 5% glycerol and 0.5 mM DTT).

6. RNA-seq analysis

6.1. Samples preparation, RNA extraction and library preparation.

Bacterial pellet samples (untreated and treated- 0.35% [v/v] MMS, 30 min) were submitted to Axil Scientific NGS, SG. Total RNA extraction was performed using the total RNA purification kit from Norgen Biotek Corp. The quality and quantity of RNA were measured using Nanodrop and Tapestation 4200. Library was prepped using Ribo-zero bacteria and mRNA library prep kit according to the manufacturer's instructions.

6.2. Sequencing and analysis

Next, the libraries were sequenced on HiSeq4K machine. Raw sequencing data were received in FASTQ formatted file. Quality control steps were performed using fastp v0.19.4 (Chen, Zhou, Chen, & Gu, 2018) to access bases quality of each sequences and also to filter low quality bases (Phred 33 quality < Q20) and adapter sequences. By using BWA v7.6 (Li & Durbin, 2009) tool, quality filtered sequences were then mapped to *Escherichia coli* BW251153 (WT) reference genome (accession number: CP009273) obtained from GenBank.

The RNA-seq generated 6.6-104.9 million raw reads with a remaining 5.8-92. 5 million clean reads that were subsequently mapped to *E. coli* genome. 5.8-91.3 million were mapped with a mapped fraction of 94.4-100% (Supplementary table 7). Resulting alignment files of each samples were used in downstream analysis of differential expression. The expression of the mRNA were then quantified using StringTie (Pertea et al., 2015) tool. Three expression values were computed which are reads count, FPKM (fragments per kilobase million) and TPM (transcripts per kilobase million). Differential expression (DE) analysis was performed using DESeq2 tool to compare expression levels of all mRNA under different experimental conditions and the expression fold change between each comparison group was calculated and log-transformed. mRNA with expression fold change ≥2 and p-adjusted <0.01 were selected as statistically significant differentially expressed.

7. RT-qPCR analysis

Bacteria were grown and treated with MMS or MMS+ α-KG as in RNA-seq experiment. Total RNA was isolated using a zymo Quick-RNA Miniprep Kit (R1055). Samples of 1µg total RNA were reverse transcribed to cDNA using iScript^{TM} Reverse Transcription supermix for RT-qPCR (Bio-Rad 1708841) according to manufacturer's instructions. cDNA samples were PCR

amplified using iTaq™ Universal SYBR Green Supermix (Bio-Rad 1725121). Real-time quantitative PCR was carried out on the ABI 7500 Fast Real-Time PCR System (Applied Biosystems).

8. AlkB in vitro demethylation assay

AlkB demethylation activity was measured by two previously described methods (Shivange et al., 2014; Shivange et al., 2016). For both methods 40 µg of chemically synthesized oligonucleotides (IDT) that contains the restriction site for the methylation sensitive restriction enzyme MboI (underlined) was used 5'-GGATGCCTTC GACACCTAGC TTTGTTAGGT CTGGATCCTC GAAATACAAA GATTGTACTG AGAGTGCACC-3'). The oligonucleotides were treated with MMS buffer (5% (v/v) MMS, 50% EtoH in a final volume of 500 µl in presence of 200 mM K_2HPO_4 at room temperature for 16 hours), dialyzed in TE buffer (10 mM Tris pH 8.0, 1 mM EDTA pH 8.0 [Sigma Aldrich E5134-50G]) using Spectra/Por dialysis membrane (MWCO: 3500) and precipitated with 2 volumes of ice cold 100% EtoH and 0.3M sodium acetate pH 5.5, washed twice with 70% EtoH and dissolved in DNase/RNase free water.

8.1 Immunoprecipitation of FLAG tagged AlkB-

AlkB was expressed in *E. coli* BL21 and Immunoprecipitated using FLAGIPT1 kit (sigma Aldrich) according to manufacturer's instructions, and Flag-AlkB proteins were eluted using a Flag peptide.

8.2 Direct fluorescence-based formaldehyde detection

This assay was performed as previously described (Shivange et al., 2016). Repair reactions (50 µl) were carried out at 37◦C for 1 hour in the presence of 1 µM AlkB, 0.5 µg (1 µM) methylated oligonucleotide and reaction buffer (20 mM Tris–HCl pH 8.0, 200 µM indicated metabolite [αKG acid, succinic acid, fumaric acid and malic acid], 2 mM L-Ascorbate and 20 µM $Fe(NH_4)_2(SO_4)_2$). Formaldehyde release was detected by mixing demethylation repair reaction product with 40 µl of 5 M ammonium acetate and 10 µl of 0.5 M acetoacetanilide to make the final volume 100 µl. The fluorescent compound was allowed to develop at room temperature for 15 min and then entire reaction mixture was transferred to 96-well microplate and analysed using a multimode reader setting the excitation wavelength at 365 nm and

emission wavelength at 465 nm. Formaldehyde standard curve was prepared by selecting a range of pure formaldehyde concentrations from 2 to 20 µM.

8.3 Restriction based demethylation assay

This assay was performed as previously described (Shivange et al., 2014). Repair reactions (50 µl) were carried out at 37°C for 4 hours in the presence of 1 µM AlkB, 0.5 µg (1 µM) methylated oligonucleotide and reaction buffer (20 mM Tris–HCl pH 8.0, 200 µM indicated metabolite, 2 mM L-Ascorbate and 20 µM $Fe(NH_4)_2(SO_4)_2$). Repair reaction oligonucleotide was annealed to equi-molar complimentary ssDNA to generate methylated dsDNA in annealing buffer (50 mM Hepes pH 8 and 10 mM EDTA pH 8) at 37°C for 60 min. repaired dsDNA was digested by MboI restriction enzyme (2 hours at 37°C followed by heat inactivation). Digestion products were dissolved on 3% agarose containing SafeU (SYBR™ Safe DNA Gel Stain, Thermo Fisher Scientific, #S33102) with 10 mM sodium borate as electrophoresis buffer at 300 V for 20 min, and visualized using Gel Documentation System (Bio Rad).

9. Western blot analysis

E. coli cells were harvested in lysis buffer containing: 50 mM Tris pH 8, 10% glycerol, 0.1% triton, 100 mM PMSF (Sigma Aldrich 10837091001), 0.1 mg/ml Lysozyme (Sigma Aldrich 10837059001). Protein concentrations were determined using the Bradford method (Kruger, 1994). Loading amount on gels was normalized using protein concentration and verified by recording the gels using Ponceau S staining. Samples were separated on 10% SDS-PAGE gels, transferred onto PVDF membranes (Millipore). The following primary antibodies were used: polyclonal anti FumA, polyclonal anti FumC and for identification of Class-I FH polyclonal anti FumB that recognizes both FumA and FumB (prepared in our lab).

S. Cerevisiae cells were harvested in lysis buffer containing: 10 mM Tris pH 8, 1 mM EDTA and 100 mM PMSF. Protein concentrations were determined using the Bradford method (Bradford, 1976). Samples were separated on 10% SDS-PAGE gels, transferred onto PVDF membranes (Millipore). The following primary antibodies were used: monoclonal anti FLAG (Sigma- F3165) and polyclonal anti Aconitase (prepared in our lab). All blots were incubated

with the appropriate IgG-HRP-conjugated secondary antibody. Protein bands were visualized and developed using ECL immunoblotting detection system (ImageQuant LAS 4000 mini GE Healthcare) and Gel Documentation System (Bio Rad).

10. Statistical analysis

Statistical analysis was conducted with the two-tailed unpaired Student's t-test. All data represent the mean ± standard error of three independent experiments.

Additional information

Acknowledgments

Funding

This work was supported by grants to Ophry Pines from the Israel Science Foundation (ISF, grant number 1455/17), the German Israeli Project Cooperation (DIP, grant number P17516) and The CREATE Project of the National Research Foundation of Singapore (SHARE MMID2). The funders had no role in study design, data collection and interpretation, or the decision to submit the work for publication.

References:

Akiba, T., Hiraga, K., & Tuboi, S. (1984). Intracellular distribution of fumarase in various animals. *J Biochem, 96*(1), 189-195. doi:10.1093/oxfordjournals.jbchem.a134812

Ashburner, M., Ball, C. A., Blake, J. A., Botstein, D., Butler, H., Cherry, J. M., . . . Sherlock, G. (2000). Gene ontology: tool for the unification of biology. The Gene Ontology Consortium. *Nat Genet, 25*(1), 25-29. doi:10.1038/75556

Ashkenazy, H., Abadi, S., Martz, E., Chay, O., Mayrose, I., Pupko, T., & Ben-Tal, N. (2016). ConSurf 2016: an improved methodology to estimate and visualize evolutionary conservation in macromolecules. *Nucleic Acids Res, 44*(W1), W344-350. doi:10.1093/nar/gkw408

Baharoglu, Z., & Mazel, D. (2014). SOS, the formidable strategy of bacteria against aggressions. *FEMS Microbiol Rev, 38*(6), 1126-1145. doi:10.1111/1574-6976.12077

Ben-Menachem, R., Wang, K., Marcu, O., Yu, Z., Lim, T. K., Lin, Q., . . . Pines, O. (2018). Yeast aconitase mitochondrial import is modulated by interactions of its C and N terminal domains and Ssa1/2 (Hsp70). *Sci Rep, 8*(1), 5903. doi:10.1038/s41598-018-24068-w

Bohnuud, T., Jones, G., Schueler-Furman, O., & Kozakov, D. (2017). Detection of Peptide-Binding Sites on Protein Surfaces Using the Peptimap Server. *Methods Mol Biol, 1561*, 11-20. doi:10.1007/978-1-4939-6798-8_2

Bradford, M. M. (1976). A rapid and sensitive method for the quantitation of microgram quantities of protein utilizing the principle of protein-dye binding. *Analytical biochemistry, 72*, 248-254. doi:10.1006/abio.1976.9999

Chen, S., Zhou, Y., Chen, Y., & Gu, J. (2018). fastp: an ultra-fast all-in-one FASTQ preprocessor. *Bioinformatics, 34*(17), i884-i890. doi:10.1093/bioinformatics/bty560

Datsenko, K. A., & Wanner, B. L. (2000). One-step inactivation of chromosomal genes in Escherichia coli K-12 using PCR products. *Proc Natl Acad Sci U S A, 97*(12), 6640-6645. doi:10.1073/pnas.120163297

Dik, E., Naamati, A., Asraf, H., Lehming, N., & Pines, O. (2016). Human Fumarate Hydratase Is Dual Localized by an Alternative Transcription Initiation Mechanism. *Traffic, 17*(7), 720-732. doi:10.1111/tra.12397

Errol, C. F., Graham, C. W., Wolfram, S., Richard, D. W., Roger, A. S., & Tom, E. (2006). *DNA Repair and Mutagenesis, Second Edition*: American Society of Microbiology.

Falnes, P. O., Klungland, A., & Alseth, I. (2007). Repair of methyl lesions in DNA and RNA by oxidative demethylation. *Neuroscience, 145*(4), 1222-1232. doi:10.1016/j.neuroscience.2006.11.018

Feliciano, P. R., Drennan, C. L., & Nonato, M. C. (2016). Crystal structure of an Fe-S cluster-containing fumarate hydratase enzyme from Leishmania major reveals a unique protein fold. *Proc Natl Acad Sci U S A, 113*(35), 9804-9809. doi:10.1073/pnas.1605031113

The Gene Ontology Resource: 20 years and still GOing strong. (2019). *Nucleic Acids Res, 47*(D1), D330-d338. doi:10.1093/nar/gky1055

Gottlieb, E., & Tomlinson, I. P. (2005). Mitochondrial tumour suppressors: a genetic and biochemical update. *Nat Rev Cancer, 5*(11), 857-866. doi:10.1038/nrc1737

Hausinger, R. P. (2004). FeII/alpha-ketoglutarate-dependent hydroxylases and related enzymes. *Crit Rev Biochem Mol Biol, 39*(1), 21-68. doi:10.1080/10409230490440541

Jiang, Y., Qian, X., Shen, J., Wang, Y., Li, X., Liu, R., . . . Lu, Z. (2018). Author Correction: Local generation of fumarate promotes DNA repair through inhibition of histone H3 demethylation. *Nat Cell Biol, 20*(10), 1226. doi:10.1038/s41556-018-0074-7

Johnson, T. I., Costa, A. S. H., Ferguson, A. N., & Frezza, C. (2018). Fumarate hydratase loss promotes mitotic entry in the presence of DNA damage after ionising radiation. *Cell Death Dis, 9*(9), 913. doi:10.1038/s41419-018-0912-3

Karniely, S., Regev-Rudzki, N., & Pines, O. (2006). The presequence of fumarase is exposed to the cytosol during import into mitochondria. *J Mol Biol, 358*(2), 396-405. doi:10.1016/j.jmb.2006.02.023

Kreuzer, K. N. (2013). DNA damage responses in prokaryotes: regulating gene expression, modulating growth patterns, and manipulating replication forks. *Cold Spring Harb Perspect Biol, 5*(11), a012674. doi:10.1101/cshperspect.a012674

Kronenberg, J., Pars, K., Brieskorn, M., Prajeeth, C. K., Heckers, S., Schwenkenbecher, P., . . . Stangel, M. (2019). Fumaric Acids Directly Influence Gene Expression of Neuroprotective Factors in Rodent Microglia. *Int J Mol Sci, 20*(2). doi:10.3390/ijms20020325

Kruger, N. J. (1994). The Bradford method for protein quantitation. *Methods Mol Biol, 32*, 9-15. doi:10.1385/0-89603-268-x:9

Leshets, M., Ramamurthy, D., Lisby, M., Lehming, N., & Pines, O. (2018). Fumarase is involved in DNA double-strand break resection through a functional interaction with Sae2. *Curr Genet, 64*(3), 697-712. doi:10.1007/s00294-017-0786-4

Li, H., & Durbin, R. (2009). Fast and accurate short read alignment with Burrows-Wheeler transform. *Bioinformatics, 25*(14), 1754-1760. doi:10.1093/bioinformatics/btp324

Loenarz, C., & Schofield, C. J. (2008). Expanding chemical biology of 2-oxoglutarate oxygenases. *Nat Chem Biol, 4*(3), 152-156. doi:10.1038/nchembio0308-152

Pertea, M., Pertea, G. M., Antonescu, C. M., Chang, T. C., Mendell, J. T., & Salzberg, S. L. (2015). StringTie enables improved reconstruction of a transcriptome from RNA-seq reads. *Nat Biotechnol, 33*(3), 290-295. doi:10.1038/nbt.3122

Pollard, P. J., Briere, J. J., Alam, N. A., Barwell, J., Barclay, E., Wortham, N. C., . . . Tomlinson, I. P. (2005). Accumulation of Krebs cycle intermediates and over-expression of HIF1alpha in tumours

which result from germline FH and SDH mutations. *Hum Mol Genet, 14*(15), 2231-2239. doi:10.1093/hmg/ddi227

Pracharoenwattana, I., Zhou, W., Keech, O., Francisco, P. B., Udomchalothorn, T., Tschoep, H., . . . Smith, S. M. (2010). Arabidopsis has a cytosolic fumarase required for the massive allocation of photosynthate into fumaric acid and for rapid plant growth on high nitrogen. *Plant J, 62*(5), 785-795. doi:10.1111/j.1365-313X.2010.04189.x

Regev-Rudzki, N., Yogev, O., & Pines, O. (2008). The mitochondrial targeting sequence tilts the balance between mitochondrial and cytosolic dual localization. *J Cell Sci, 121*(Pt 14), 2423-2431. doi:10.1242/jcs.029207

Sass, E., Karniely, S., & Pines, O. (2003). Folding of fumarase during mitochondrial import determines its dual targeting in yeast. *J Biol Chem, 278*(46), 45109-45116. doi:10.1074/jbc.M302344200

Sciacovelli, M., & Frezza, C. (2017). Fumarate drives EMT in renal cancer. *Cell Death Differ, 24*(1), 1-2. doi:10.1038/cdd.2016.137

Sciacovelli, M., Goncalves, E., Johnson, T. I., Zecchini, V. R., da Costa, A. S., Gaude, E., . . . Frezza, C. (2016). Corrigendum: Fumarate is an epigenetic modifier that elicits epithelial-to-mesenchymal transition. *Nature, 540*(7631), 150. doi:10.1038/nature20144

Selak, M. A., Armour, S. M., MacKenzie, E. D., Boulahbel, H., Watson, D. G., Mansfield, K. D., . . . Gottlieb, E. (2005). Succinate links TCA cycle dysfunction to oncogenesis by inhibiting HIF-alpha prolyl hydroxylase. *Cancer Cell, 7*(1), 77-85. doi:10.1016/j.ccr.2004.11.022

Shivange, G., Kodipelli, N., & Anindya, R. (2014). A nonradioactive restriction enzyme-mediated assay to detect DNA repair by Fe(II)/2-oxoglutarate-dependent dioxygenase. *Anal Biochem, 465*, 35-37. doi:10.1016/j.ab.2014.07.003

Shivange, G., Monisha, M., Nigam, R., Kodipelli, N., & Anindya, R. (2016). RecA stimulates AlkB-mediated direct repair of DNA adducts. *Nucleic Acids Res, 44*(18), 8754-8763. doi:10.1093/nar/gkw611

Singer, E., Silas, Y. B., Ben-Yehuda, S., & Pines, O. (2017). Bacterial fumarase and L-malic acid are evolutionary ancient components of the DNA damage response. *Elife, 6*. doi:10.7554/eLife.30927

Tahiliani, M., Koh, K. P., Shen, Y., Pastor, W. A., Bandukwala, H., Brudno, Y., . . . Rao, A. (2009). Conversion of 5-methylcytosine to 5-hydroxymethylcytosine in mammalian DNA by MLL partner TET1. *Science, 324*(5929), 930-935. doi:10.1126/science.1170116

Tuboi, S., Suzuki, T., Sato, M., & Yoshida, T. (1990). Rat liver mitochondrial and cytosolic fumarases with identical amino acid sequences are encoded from a single mRNA with two alternative in-phase AUG initiation sites. *Adv Enzyme Regul, 30*, 289-304. doi:10.1016/0065-2571(90)90023-u

van Vugt-Lussenburg, B. M., van der Weel, L., Hagen, W. R., & Hagedoorn, P. L. (2013). Biochemical similarities and differences between the catalytic [4Fe-4S] cluster containing fumarases FumA and FumB from Escherichia coli. *PLoS One, 8*(2), e55549. doi:10.1371/journal.pone.0055549

Woods, S. A., Schwartzbach, S. D., & Guest, J. R. (1988). Two biochemically distinct classes of fumarase in Escherichia coli. *Biochim Biophys Acta, 954*(1), 14-26. doi:10.1016/0167-4838(88)90050-7

Xiao, M., Yang, H., Xu, W., Ma, S., Lin, H., Zhu, H., . . . Guan, K. L. (2012). Inhibition of alpha-KG-dependent histone and DNA demethylases by fumarate and succinate that are accumulated in mutations of FH and SDH tumor suppressors. *Genes Dev, 26*(12), 1326-1338. doi:10.1101/gad.191056.112

Yang, J., Yan, R., Roy, A., Xu, D., Poisson, J., & Zhang, Y. (2015). The I-TASSER Suite: protein structure and function prediction. *Nat Methods, 12*(1), 7-8. doi:10.1038/nmeth.3213

Yogev, O., Yogev, O., Singer, E., Shaulian, E., Goldberg, M., Fox, T. D., & Pines, O. (2010). Fumarase: a mitochondrial metabolic enzyme and a cytosolic/nuclear component of the DNA damage response. *PLoS Biol, 8*(3), e1000328. doi:10.1371/journal.pbio.1000328

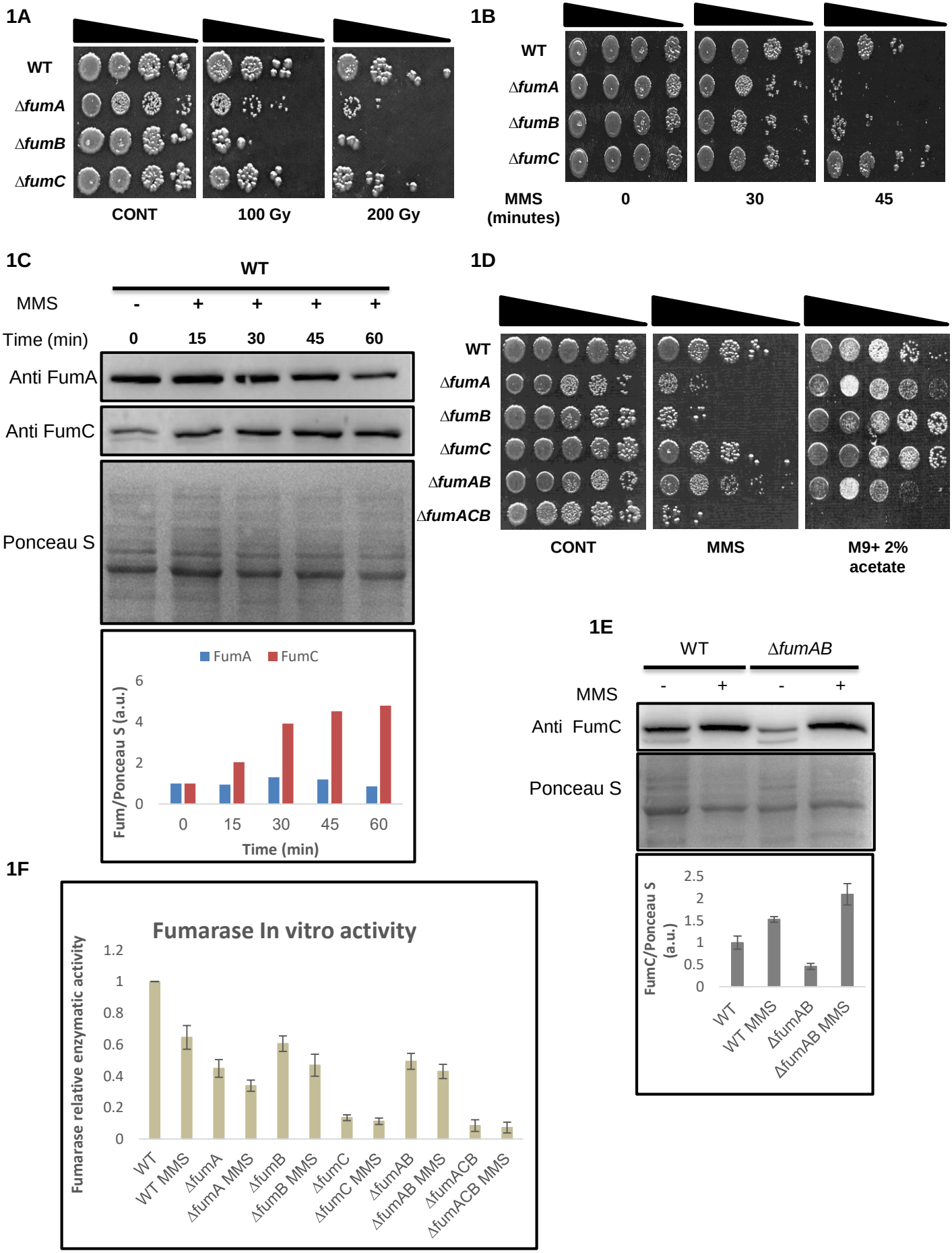
1A
WT
ΔfumA
ΔfumB
ΔfumC
CONT
100 Gy
200 Gy
1B
WT
ΔfumA
ΔfumB
ΔfumC
MMS (minutes)
0
30
45
1C
WT
MMS
- + + + +
Time (min)
0 15 30 45 60
Anti FumA
Anti FumC
Ponceau S
FumA
FumC
Fum/Ponceau S (a.u.)
0 2 4 6
0 15 30 45 60
Time (min)
1D
WT
ΔfumA
ΔfumB
ΔfumC
ΔfumAB
ΔfumACB
CONT
MMS
M9+ 2% acetate
1E
WT
ΔfumAB
MMS
- + - +
Anti FumC
Ponceau S
FumC/Ponceau S (a.u.)
0 0.5 1 1.5 2 2.5
WT
WT MMS
ΔfumAB
ΔfumAB MMS
1F
Fumarase In vitro activity
Fumarase relative enzymatic activity
0 0.2 0.4 0.6 0.8 1 1.2
WT
WT MMS
ΔfumA
ΔfumA MMS
ΔfumB
ΔfumB MMS
ΔfumC
ΔfumC MMS
ΔfumAB
ΔfumAB MMS
ΔfumACB
ΔfumACB MMS

Figure 1- *E. coli* FumA and FumB are required for DNA damage repair. (**A, B**) *E. coli* wild type (WT), *ΔfumA*, *ΔfumB*, *ΔfumC*, strains were irradiated or treated with MMS (0.35% (v/v) for 45 minutes at 37°C) respectively. The cells were then washed and serially diluted (spot test) onto LB plates. (**C**) *E. coli* wild type (WT) was treated with MMS (0.35% [v/v] for 45 minutes at 37°C), the cells were lysed and centrifuged to obtain a supernatant which was subjected to Western blotting (using the indicated antibodies) and Ponceau S staining. The chart presents the relative amount of FumA and FumC with or without MMS according to densitometric analysis of Fig. 1C and normalized to Ponceau S staining (**D**) *E. coli* strains were grown and subjected to spot assay as in Fig. 1B (n=3, for all spot test assays) (**E**) *E. coli* WT and *ΔfumAB* were grown as in (**B,** 0.35% MMS (v/v) for 45 min) and subjected to protein extraction and Western blotting. The chart presents the relative amount of FumC with or without MMS according to densitometric analysis of Fig. 1E and normalized to Ponceau S staining (mean ±SEM [n = 3], $p<0.05$). (**F**) *E. coli* strains were grown to mid-exponential phase, the cells were lysed and centrifuged to obtain the supernatant which was assayed for fumarase activity at 250 nm with L-malic acid as the substrate (mean ± SEM [n = 3]).

Host- *S. cerevisiae*

2A

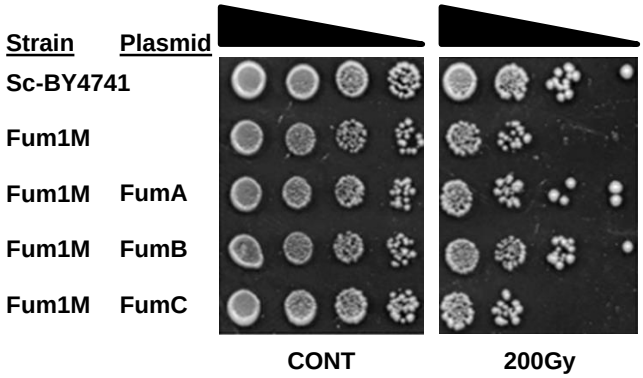

2B

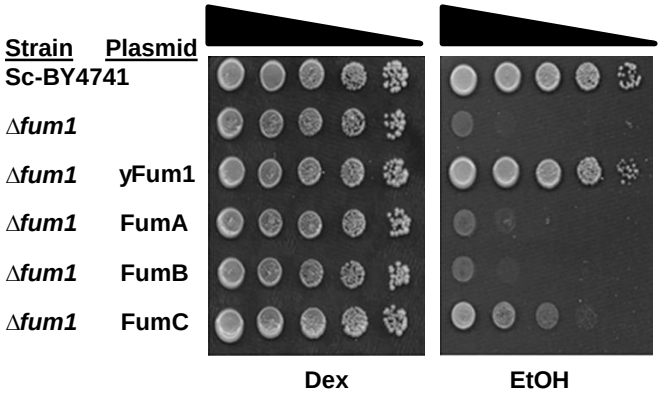

2C

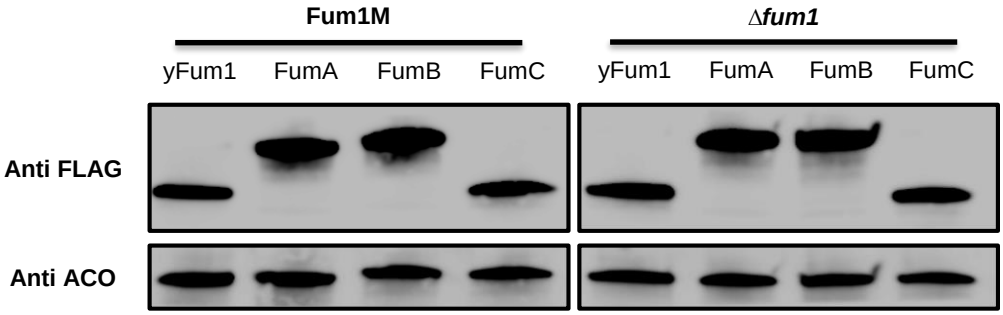

2D

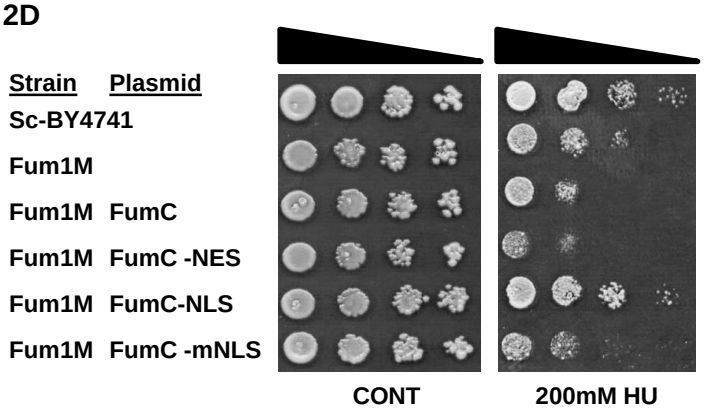

2E

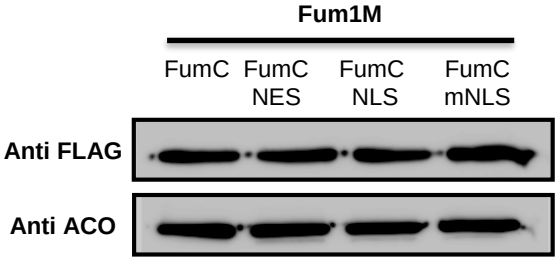

Figure 2- FumA, FumB and FumC substitute yeast Fum1 functions in the S. cerevisiae model system. (A) S. cerevisiae wild type BY4741 (Sc-BY4741), Fum1M and Fum1M harboring plasmids encoding the indicated plasmids, were grown in galactose synthetic complete (SC-Gal) medium, irradiated and serially diluted onto dextrose synthetic complete (SC-Dex) plates. (B) S. cerevisiae wild type Sc-BY4741, Δfum1 and Δfum1 strains harboring plasmids encoding the indicated plasmids, were serially diluted onto dextrose or ethanol plates. (C) Strains harboring plasmids encoding indicated proteins (yFum1, FumA, FumB, FumC) were lysed and centrifuged to obtain the supernatant, and extracts were subjected to Western blotting, using the indicated antibodies (anti Aco1 is the loading control). (D) S. cerevisiae wild type Sc-BY4741, Fum1M and Fum1M harboring plasmids encoding the indicated plasmids, were grown to exponential phase in SC-Gal medium, serially diluted (spot test) onto SC-Dex or SC-Dex + Hydroxyurea (200 mM, HU). (E) Strains harboring plasmids encoding variant recombinant fumC genes were lysed and centrifuged to obtain the supernatant, and extracts were subjected to Western blotting, using the indicated antibodies (anti Aco1 is the loading control). Each result is representative of at least three independent experiments.

3A

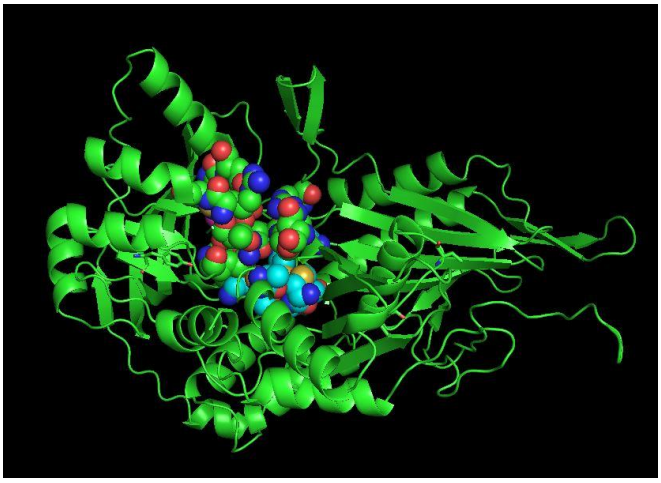

3B

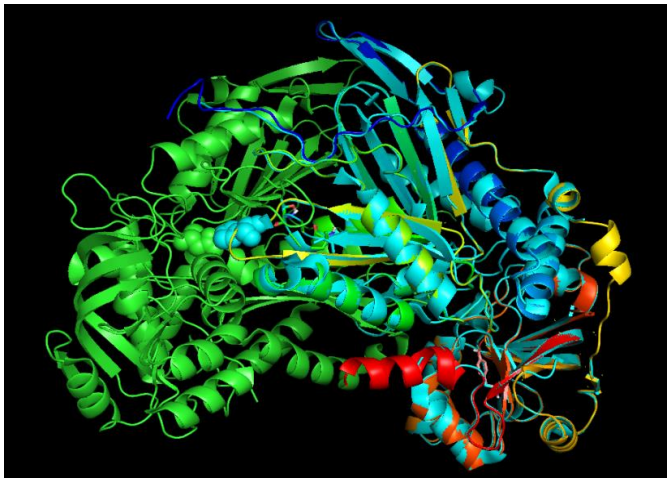

3C

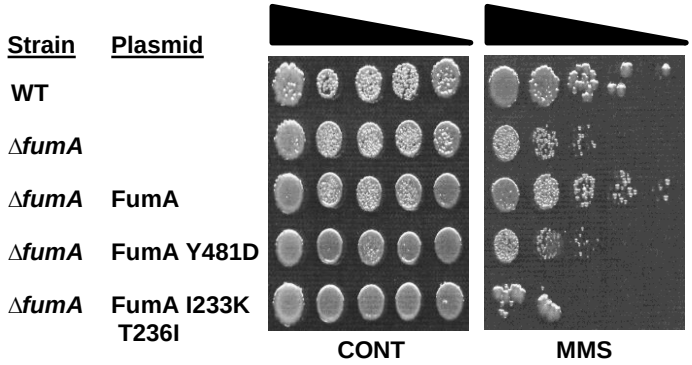

3D

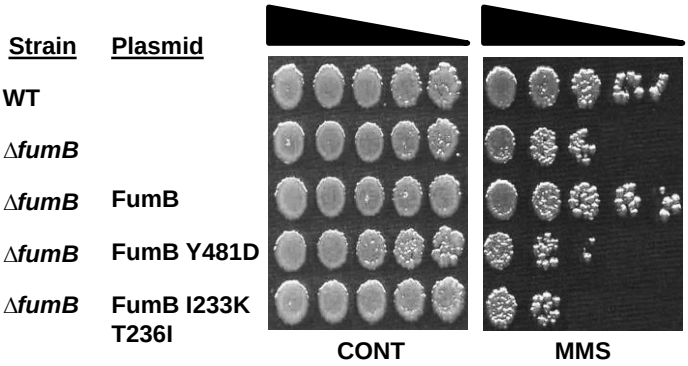

3E

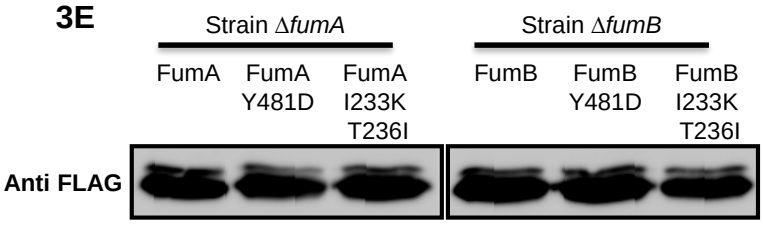

3F

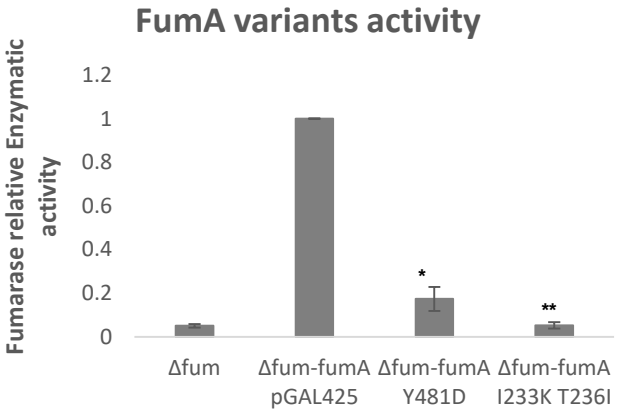

3G

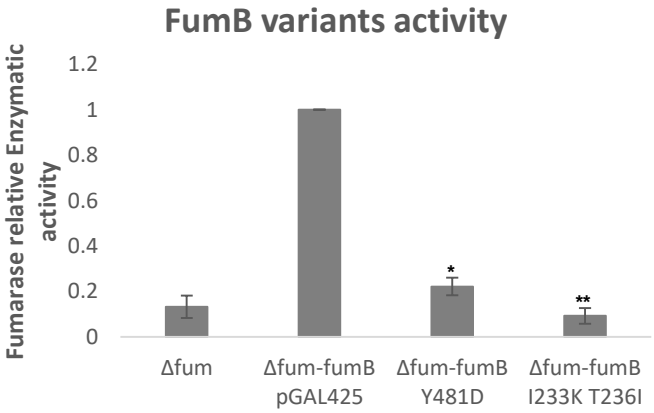

Figure 3- FumA and FumB catalytic activity is required for their DNA damage related function. (**A**) Model structure as proposed by I-TASSER, catalytic site as proposed by PEPTIMAP and homologous to *L. major* active site, and location of important amino acids for the function of this enzyme proposed by CONSURF. (**B**) Alignment of proposed FumA/FumB structure with Fumarate Hydratase of *Leishmania major.* (**C**) *E. coli* wild type (WT), *ΔfumA* and *ΔfumA* harboring the indicated plasmids. (**D**) *E. coli* wild type (WT), *ΔfumB* and *ΔfumB* harboring the indicated plasmids were grown as in Fig. 1B and subjected to spot test. (**E**) *E. coli* Δ*fumA,* Δ*fumB* harboring the indicated plasmids were grown to exponential phase, the cells were lysed and centrifuged to obtain the supernatants which were subjected to Western blotting, using the indicated antibodies. (**F, G**) *fum* null mutant harboring the indicated plasmids were grown as in Fig 3E. The cells were lysed and centrifuged to obtain the supernatant which was assayed for fumarase activity at 250 nm with L-malic acid as the substrate (mean ± SD [n = 3], two-tailed *t*-test *$p < 0.05$; **$p < 0.01$).

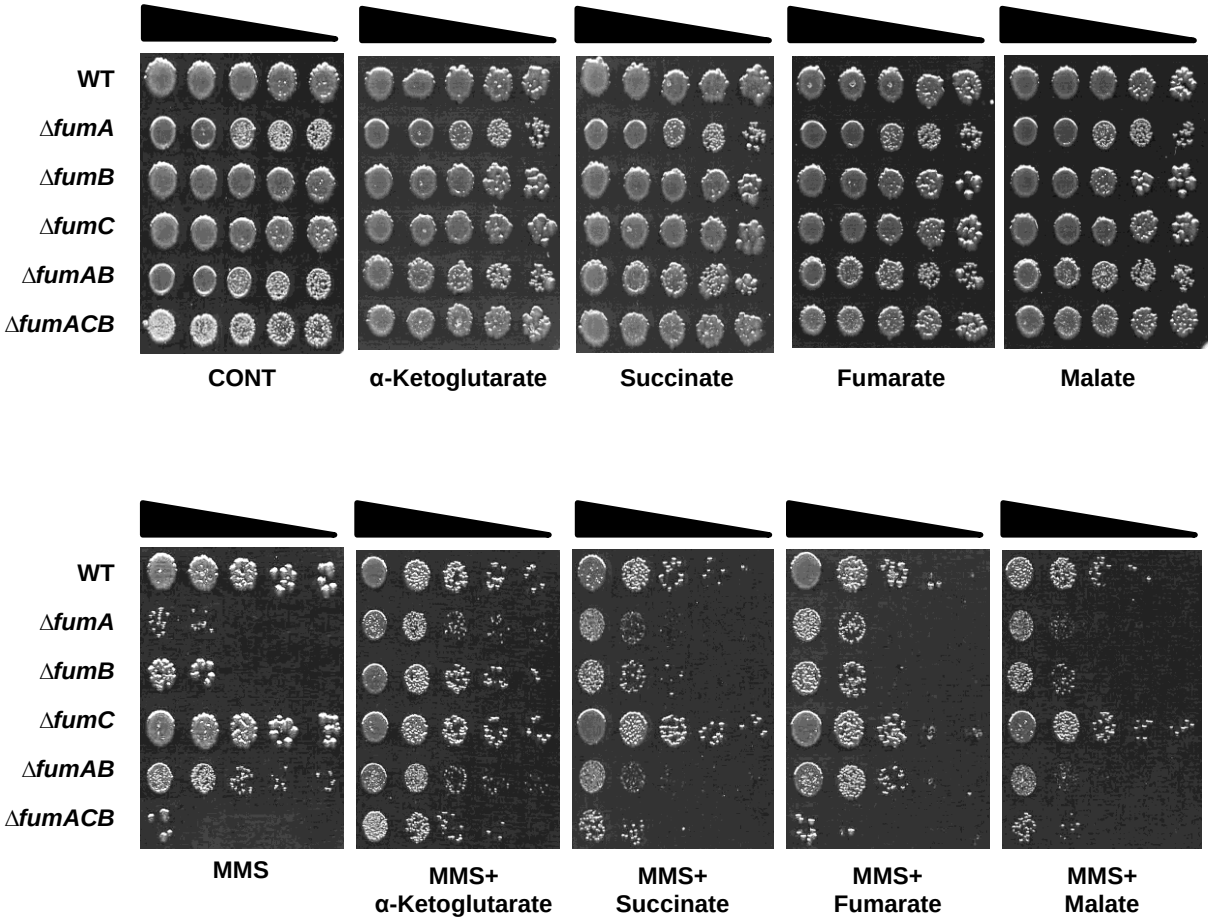

Figure 4- α-KG metabolically signal DNA repair in *fum* null mutant strains. *E. coli* wild type (WT), *ΔfumA, ΔfumB, ΔfumC*, *ΔfumAB* and *ΔfumACB* strains were grown as in Fig. 1B. The cells were serially diluted (spot test) onto LB plates containing or lacking the indicated organic acid. Each result is representative of at least three independent experiments.

Differentially expressed genes (DEGs, up and down regulated) log2FC ≥2.0

Altered expression in WT vs DNA damage sensitive *fum* null mutants

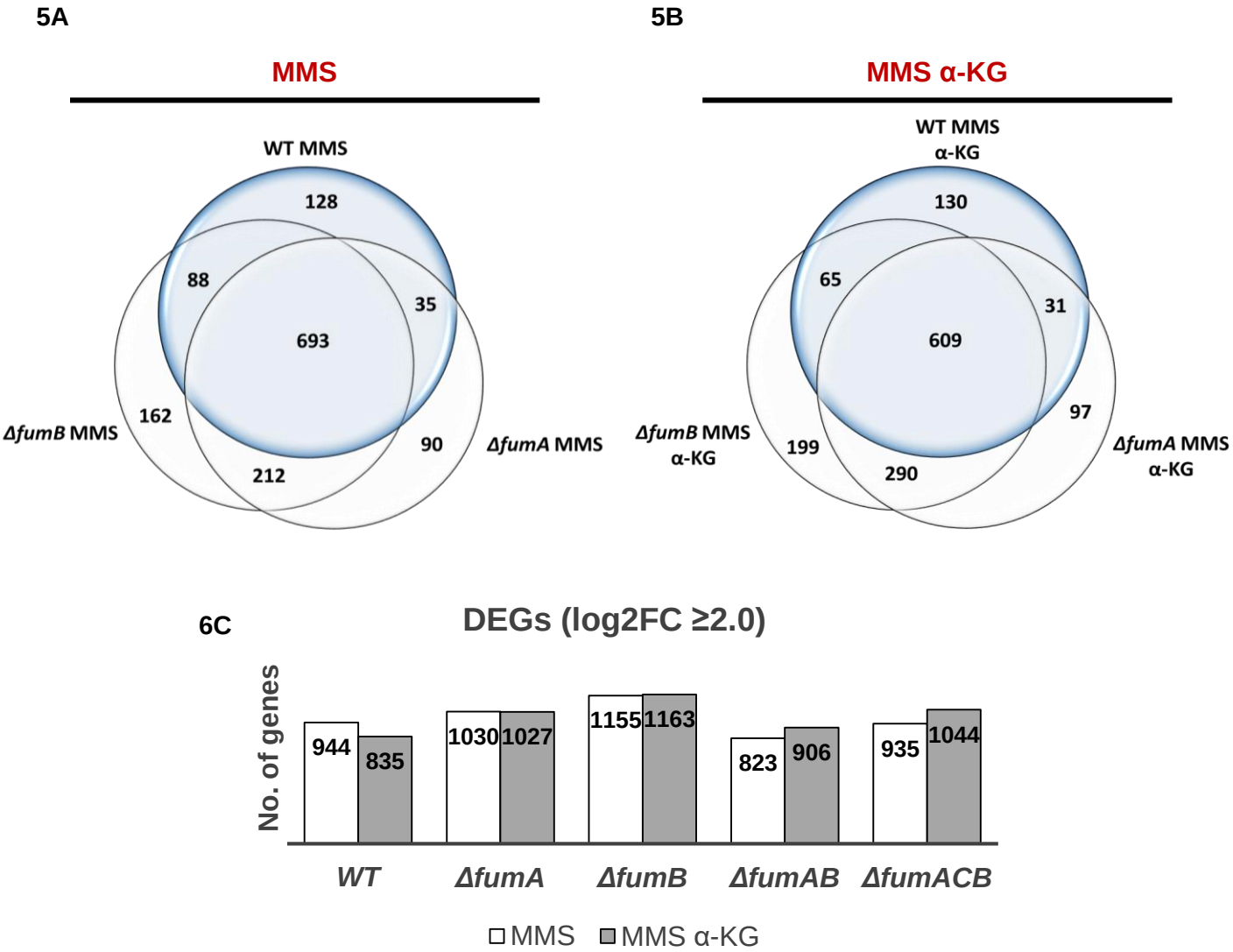

Figure 5- Absence of fumarase alters transcription in *E. coli*. RNA-seq analysis; *E. coli* wild type (WT), *ΔfumA, ΔfumB, ΔfumAB* and *ΔfumACB* strains were grown as in Fig. 1B. Cells were collected and total RNA was extracted and subjected to RNA-seq analysis (see materials and methods). (**A, B**) Venn diagrams showing the common and differential genes (transcripts) between *E. coli* wild type (WT), *ΔfumA* and *ΔfumB* strains and following treatment with MMS or MMS+25mM α-KG. (**C**) Column diagram (histogram) showing the number of differentially expressed genes in *E. coli* wild type (WT), *ΔfumA, ΔfumB*, *ΔfumAB* and *ΔfumACB.*

6A

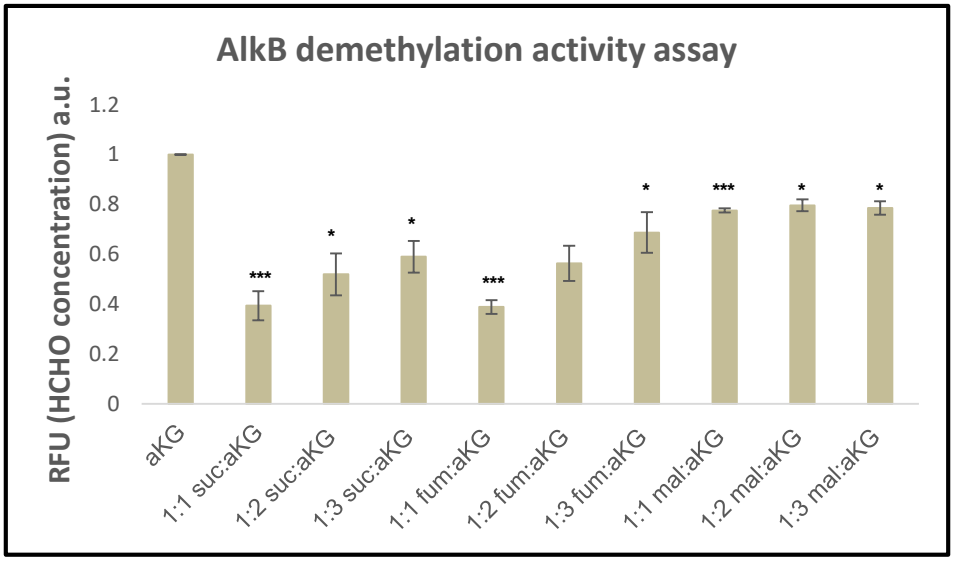
AlkB demethylation activity assay
RFU (HCHO concentration) a.u.
1.2
1
0.8
0.6
0.4
0.2
0
***
*
*
***
*
***
*
*
aKG
1:1 suc:aKG
1:2 suc:aKG
1:3 suc:aKG
1:1 fum:aKG
1:2 fum:aKG
1:3 fum:aKG
1:1 mal:aKG
1:2 mal:aKG
1:3 mal:aKG

6B

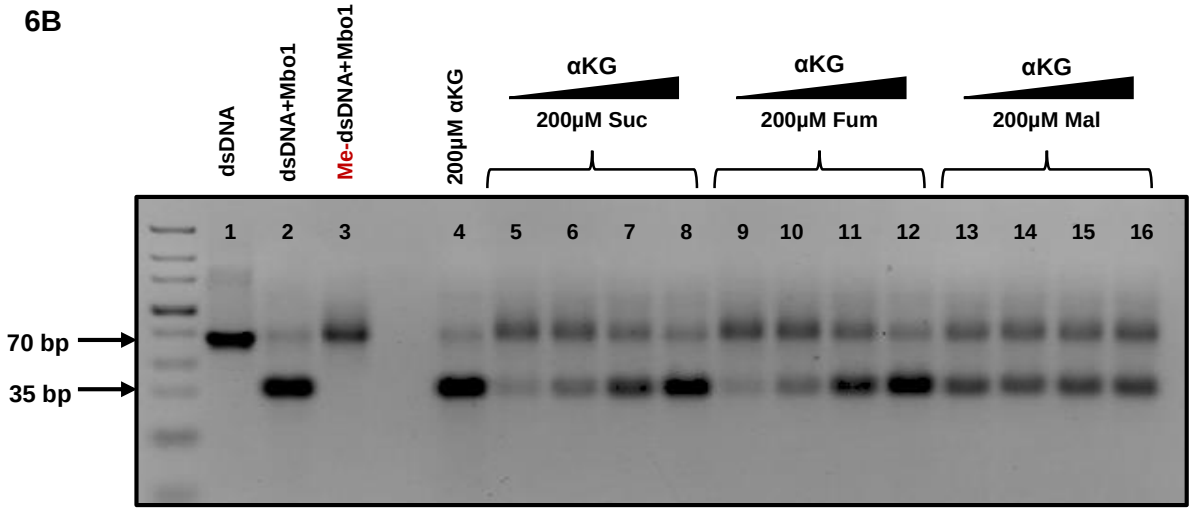
dsDNA
dsDNA+Mbo1
Me-dsDNA+Mbo1
200μM αKG
αKG
200μM Suc
αKG
200μM Fum
αKG
200μM Mal
1 2 3 4 5 6 7 8 9 10 11 12 13 14 15 16
70 bp
35 bp

6C

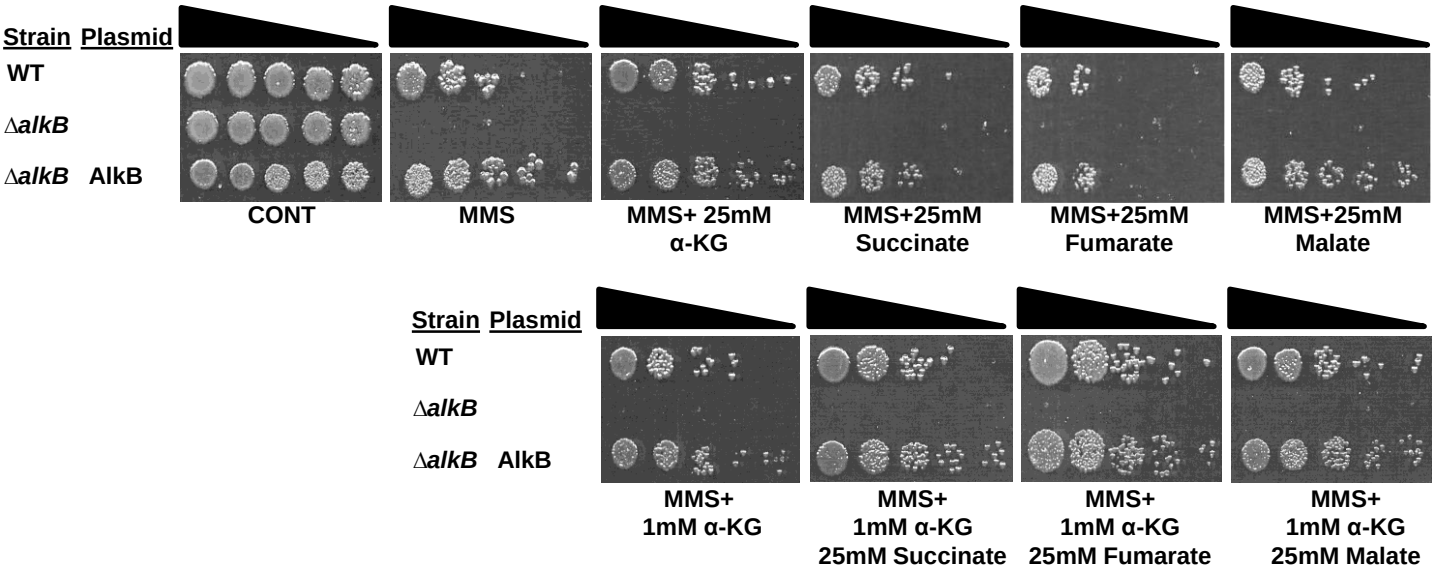
Strain Plasmid
WT
ΔalkB
ΔalkB AlkB
CONT
MMS
MMS+ 25mM α-KG
MMS+25mM Succinate
MMS+25mM Fumarate
MMS+25mM Malate
Strain Plasmid
WT
ΔalkB
ΔalkB AlkB
MMS+ 1mM α-KG
MMS+ 1mM α-KG 25mM Succinate
MMS+ 1mM α-KG 25mM Fumarate
MMS+ 1mM α-KG 25mM Malate

6D

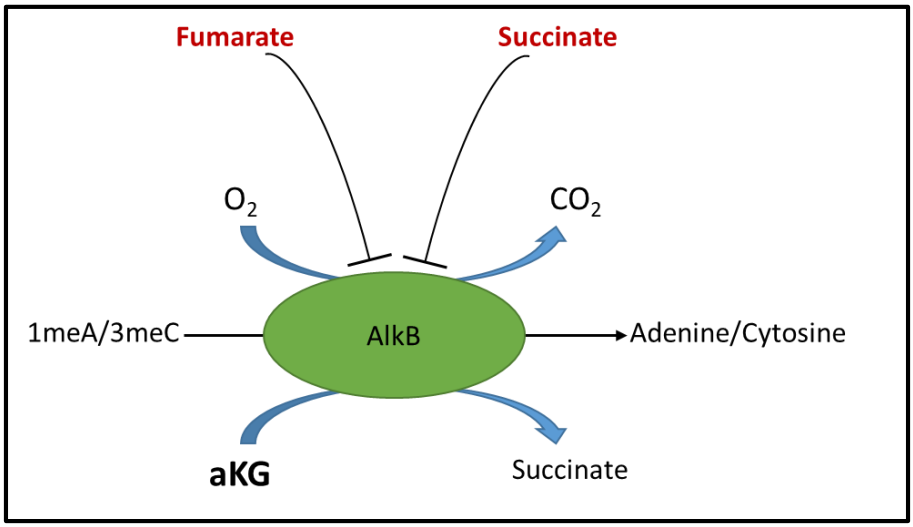

Figure 6- Fumarate and succinate inhibit AlkB demethylase activity. (**A**) Repair of methylated oligonucleotides for 1 hour at 37°C by AlkB. DNA repair was quantified by measuring formaldehyde release following mixture of the repair reaction with ammonia and acetoacetanilide forming a highly fluorescent dihydropyridine derivative. The reaction was analyzed using a multimode reader setting the excitation wavelength at 365 nm and emission wavelength at 465 nm. The graph is represented as mean ± standard error (*n=3*, two-tailed *t*-test *p < 0.05; **p < 0.01; ***p < 0.005). (**B**) Repair of methylated oligonucleotides for 4 hours at 37°C by AlkB, was detected by annealing to complementary oligonucleotides, digestion with MboI and agarose electrophoresis and staining with safeU. Following successful demethylation, digestion with MboI produced a 35bp product. (**C***) E. coli* wild type (WT), *ΔalkB* and *ΔalkB* expressing AlkB were as in Fig 1B. The cells were then washed and serially diluted (spot test) onto LB plates and LB plates containing the indicated organic acids. (**D)** Proposed model for the participation of α-KG, fumarate and succinate in the regulation of AlkB activity.

Supplemental figures

S1A

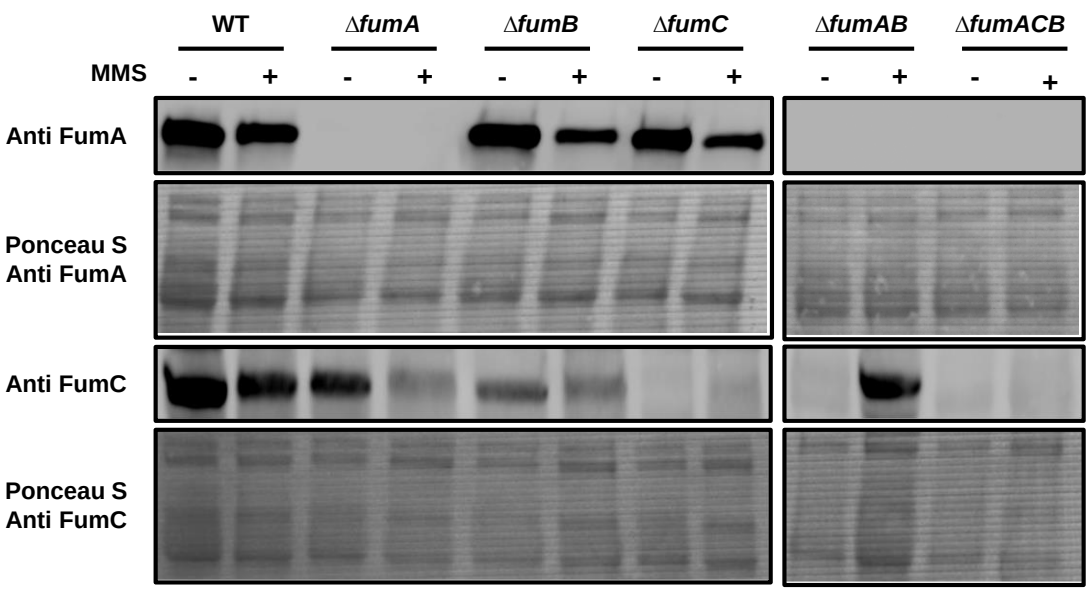
WT
ΔfumA
ΔfumB
ΔfumC
ΔfumAB
ΔfumACB
MMS
- + - + - + - + - + - +
Anti FumA
Ponceau S
Anti FumA
Anti FumC
Ponceau S
Anti FumC

S1B

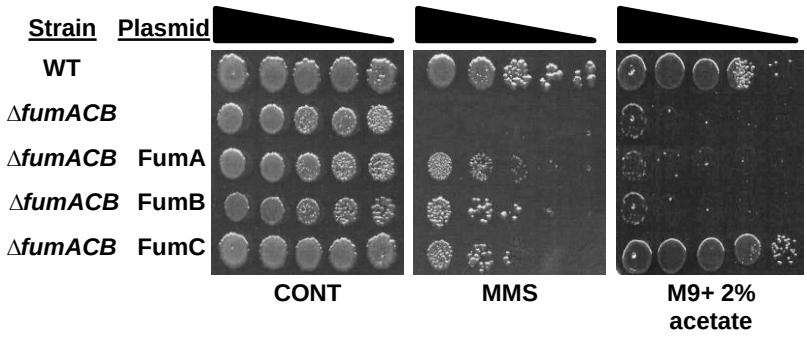
Strain
Plasmid
WT
ΔfumACB
ΔfumACB FumA
ΔfumACB FumB
ΔfumACB FumC
CONT
MMS
M9+ 2% acetate

S1C

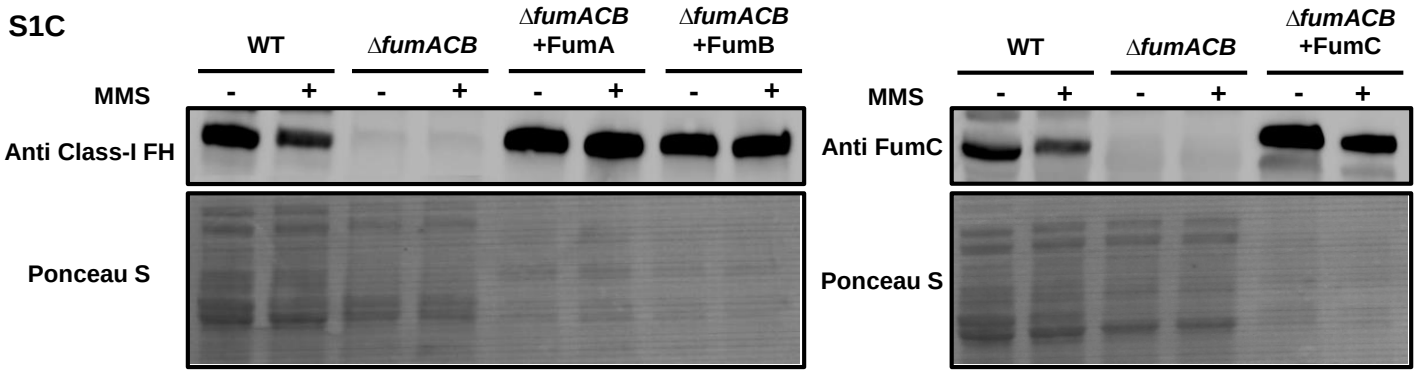
WT
ΔfumACB
ΔfumACB +FumA
ΔfumACB +FumB
MMS
- + - + - + - +
Anti Class-I FH
Ponceau S
WT
ΔfumACB
ΔfumACB +FumC
MMS
- + - + - +
Anti FumC
Ponceau S

Figure S1- In the absence of FumA and FumB, FumC participates in the DDR in *E. coli*. (**A**) *E. coli* wild type (WT), *ΔfumA*, *ΔfumB*, *ΔfumC*, *ΔfumAB, ΔfumACB* strains were grown to mid-exponential phase and irradiated to induce DSBs. The cells were then washed and serially diluted (spot test) onto LB plates. (**B**) *E. coli* wild type (WT), *ΔfumA*, *ΔfumB*, *ΔfumC*, *ΔfumAB, ΔfumACB* strains were grown to mid-exponential phase and treated with MMS (0.35% (v/v) for 45 minutes at 37°C). Total cell extracts were prepared from the indicated samples and subjected to Western blotting, using the indicated antibodies followed by Ponceau S staining. Each result is representative of three independent experiments. (**C**) *E. coli* wild type (WT), Δ*fumACB* and Δ*fumACB* harboring plasmids encoding the indicated proteins were grown to early exponential phase and MMS was added to a final concentration of 0.35% [v/v] for 45 minutes at 37°C. The cells were then washed and serially diluted (spot test) onto LB and M9+2% acetate plates. (**D**) Bacteria were grown and treated with MMS as in S1A, total cell extracts were prepared from the indicated samples and subjected to Western blotting, using the indicated antibodies followed by Ponceau S staining. Each result is representative of three independent experiments.

Host- *S. cerevisiae*

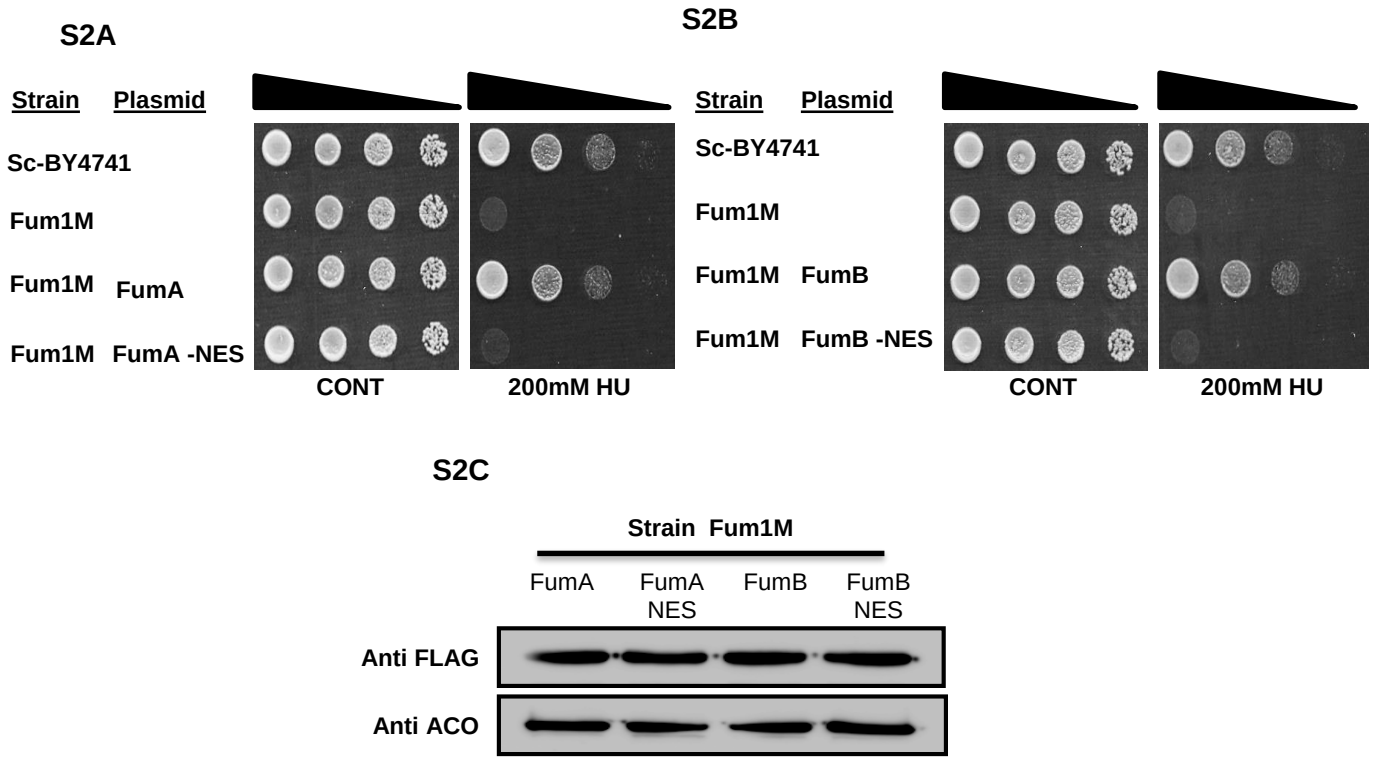

Figure S2- FumA-NES and FumB-NES do not complement DNA damage sensitivity in *S. cerevisiae*. (**A, B**) *S. cerevisiae* wild type Sc-BY4741, *Fum1M* and *Fum1M* harboring plasmids encoding the indicated proteins, were grown to exponential phase in SC-Gal medium and serially diluted onto SC-Dex or SC-Dex+ 200 mM HU. (**C**) These strains were also lysed and centrifuged to obtain the supernatant and extracts were subjected to Western blotting, using the indicated antibodies (anti Aco1 as the loading control). Each result is representative of at least three independent experiments.

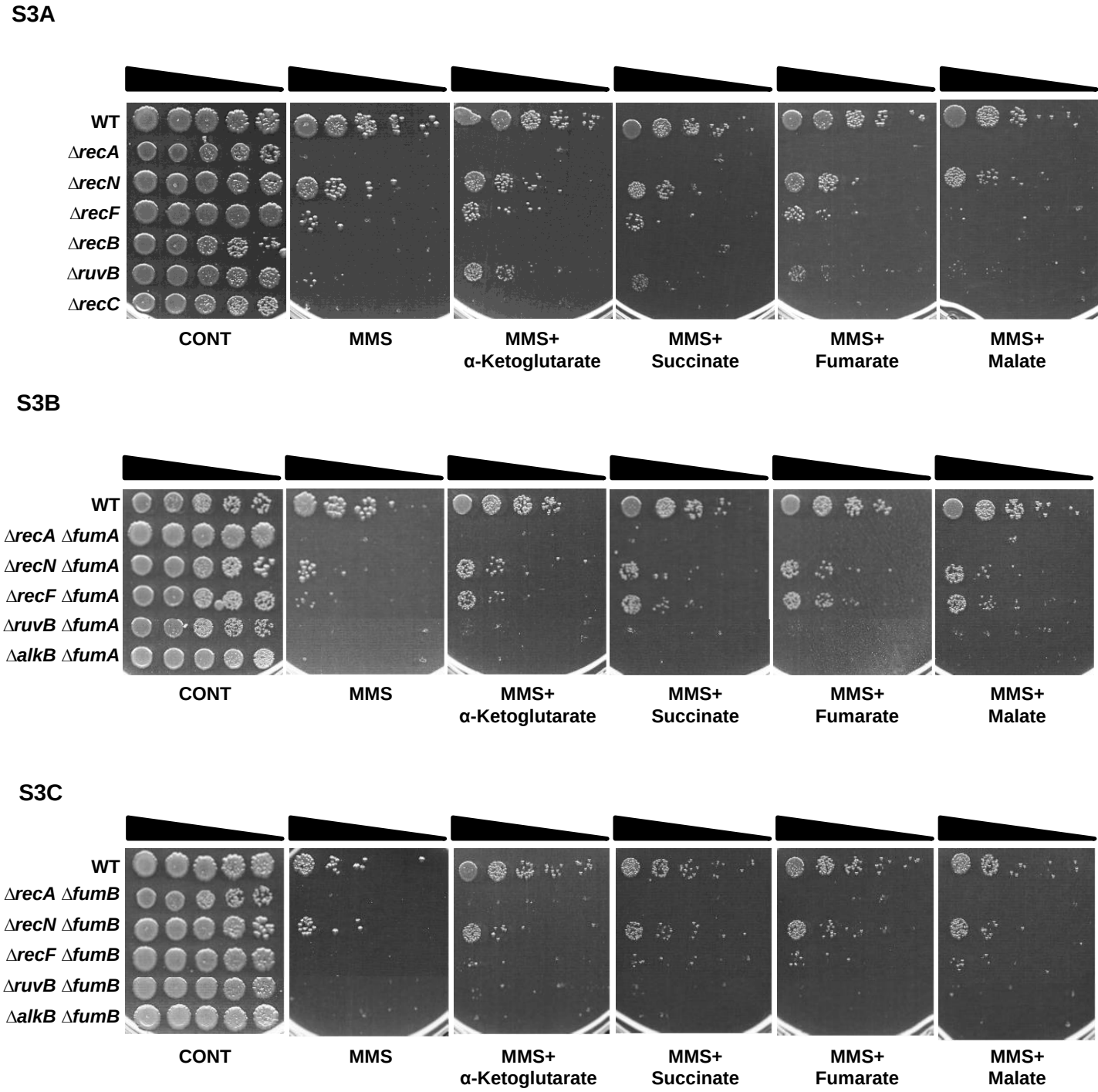

Figure S3- α-KG complementation of DNA damage sensitivity is specific to *fum* null mutants.

(**A, B, C**) *E. coli* DNA damage repair genes mutants and composite *ΔfumA*+ damage repair genes or *ΔfumB*+ damage repair genes mutants, were grown as in Fig S1A. The cells were then washed and serially diluted (spot test) onto LB agar and LB containing the indicated organic acid plates.

Differentially expressed genes (DEGs) log2FC ≥2.0

Altered expression in WT vs *fum* null mutants

S4A

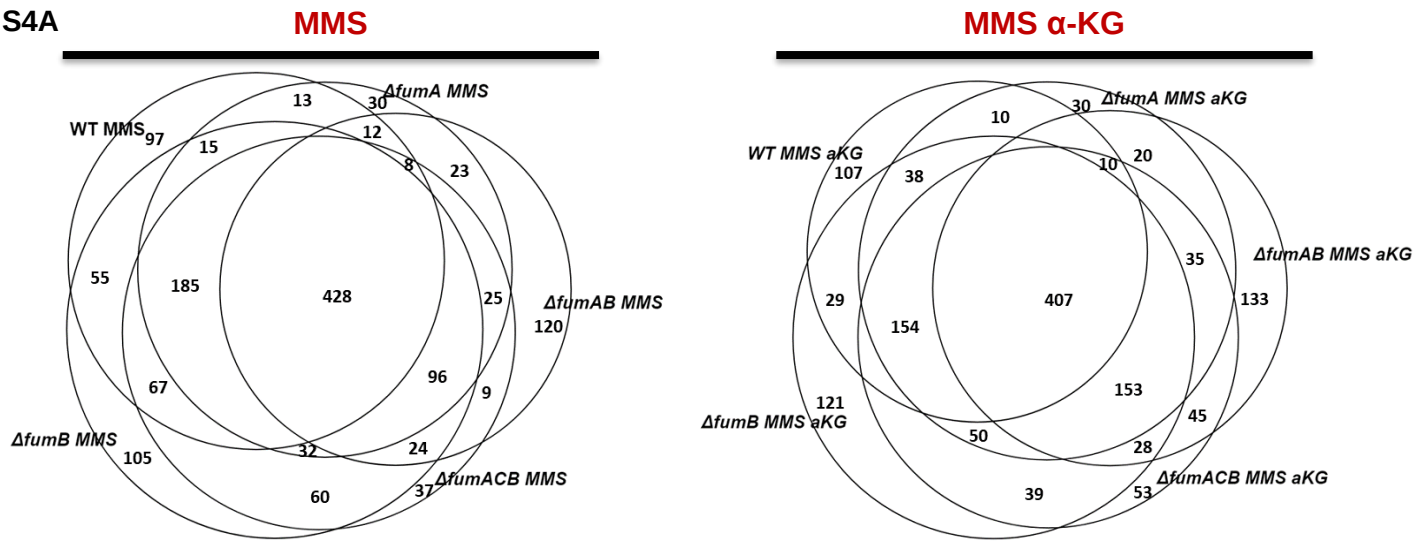

S4B

α-KG effect on DEGs

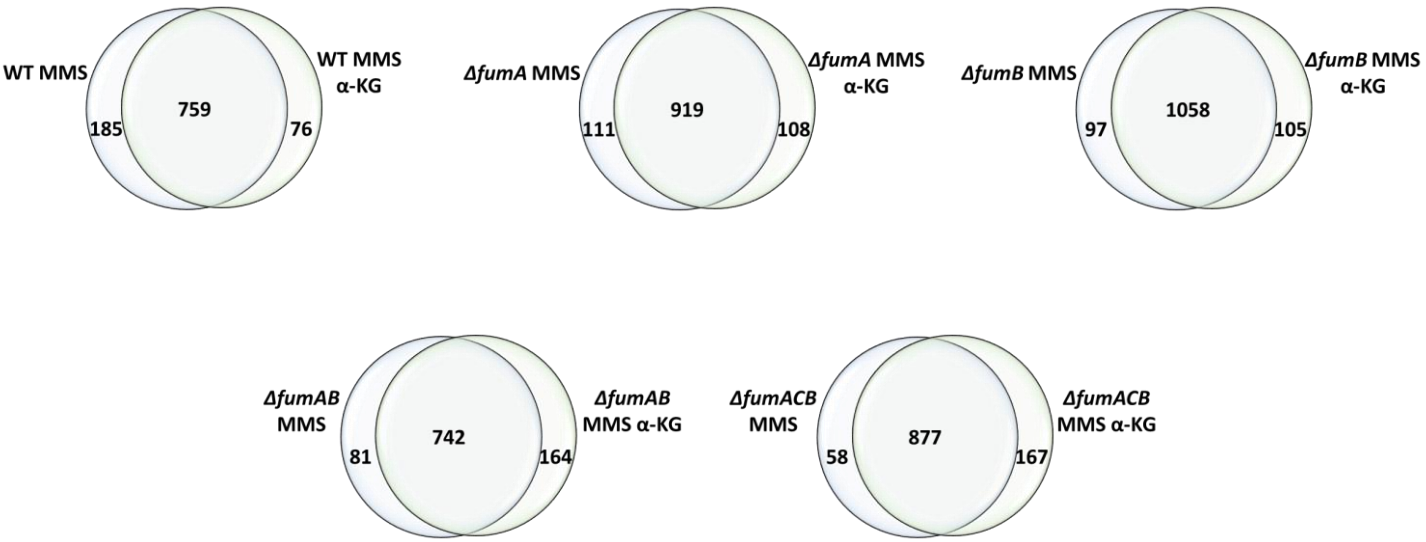

mRNA expression (RNA-seq)

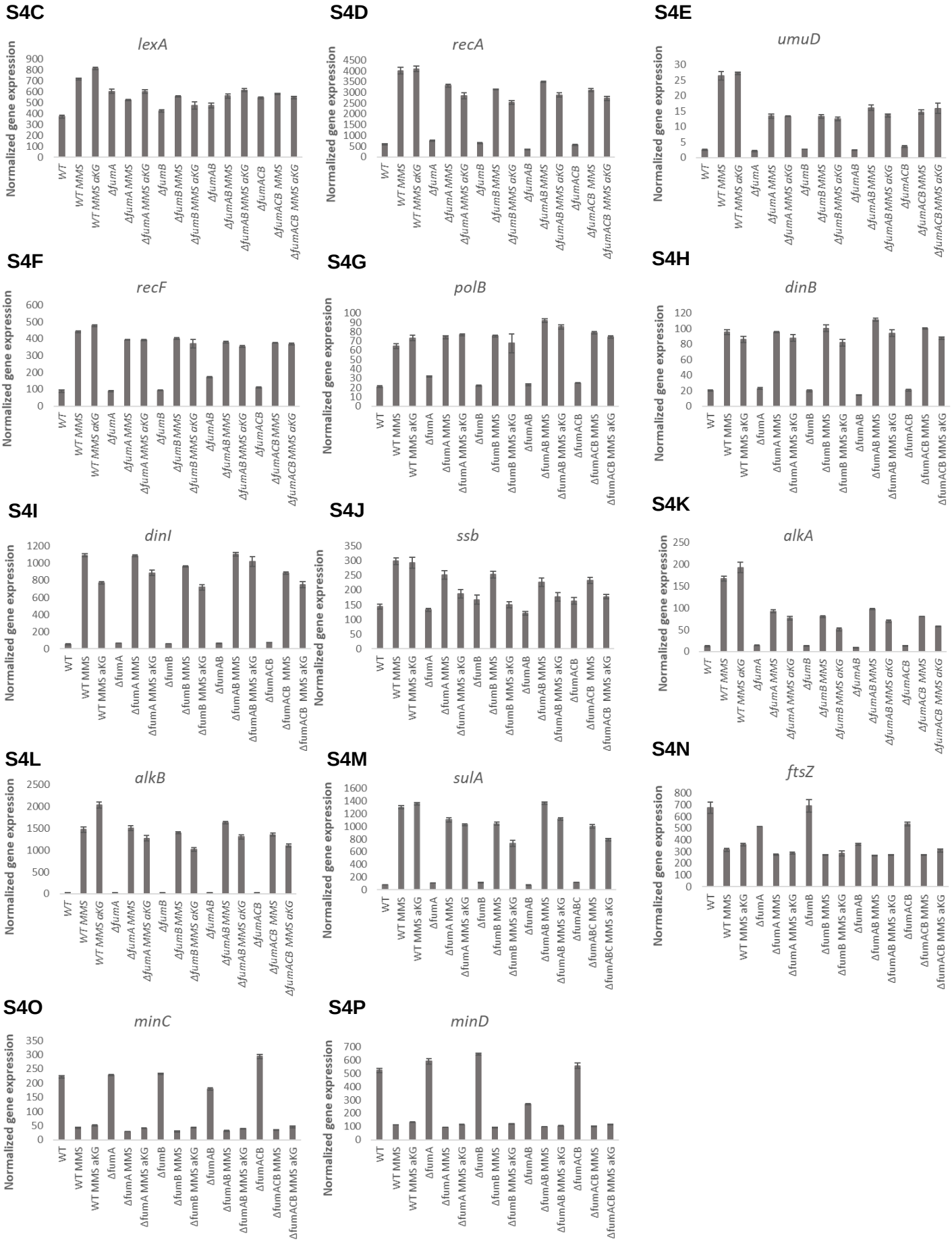

Figure S4- RNA-seq analysis of differential expressed genes. (A, B) Venn diagrams showing the common and differential genes (transcripts) between (A) E. coli wild type (WT), ΔfumA, ΔfumB, ΔfumAB and ΔfumACB strains, following treatment with MMS or MMS+25mM α-KG. (BioVinci 1.1.5, BioTuring Inc., San Diego, California, USA) (B) comparison of shared transcripts in the presence or absence of α-KG in E. coli wild type (WT), ΔfumA, ΔfumB, ΔfumAB and ΔfumACB strains. (C-P) Gene expression levels revealed by RNA-seq for (C) lexA, LexA repressor (D) recA, Protein RecA (E) umuD, Protein UmuD (F) recF, Protein RecF (G) polB, DNA polymerase II (H) dinB, DNA polymerase IV (I) dinI, DNA damage-inducible protein I (J) ssb, single-stranded DNA-binding protein (K) alkA, DNA-3-methyladenine glycosylase 2 (L) alkB, Alpha-ketoglutarate-dependent dioxygenase AlkB (M) sulA, SOS cell division inhibitor (N) ftsZ, Cell division protein FtsZ (O) minC, Septum site-determining protein MinC (P) minD, Septum site-determining protein MinD. TPM (transcripts per kilobase million) shown as Normalized gene expression from RNA-seq are mean ± standard error (n=3).

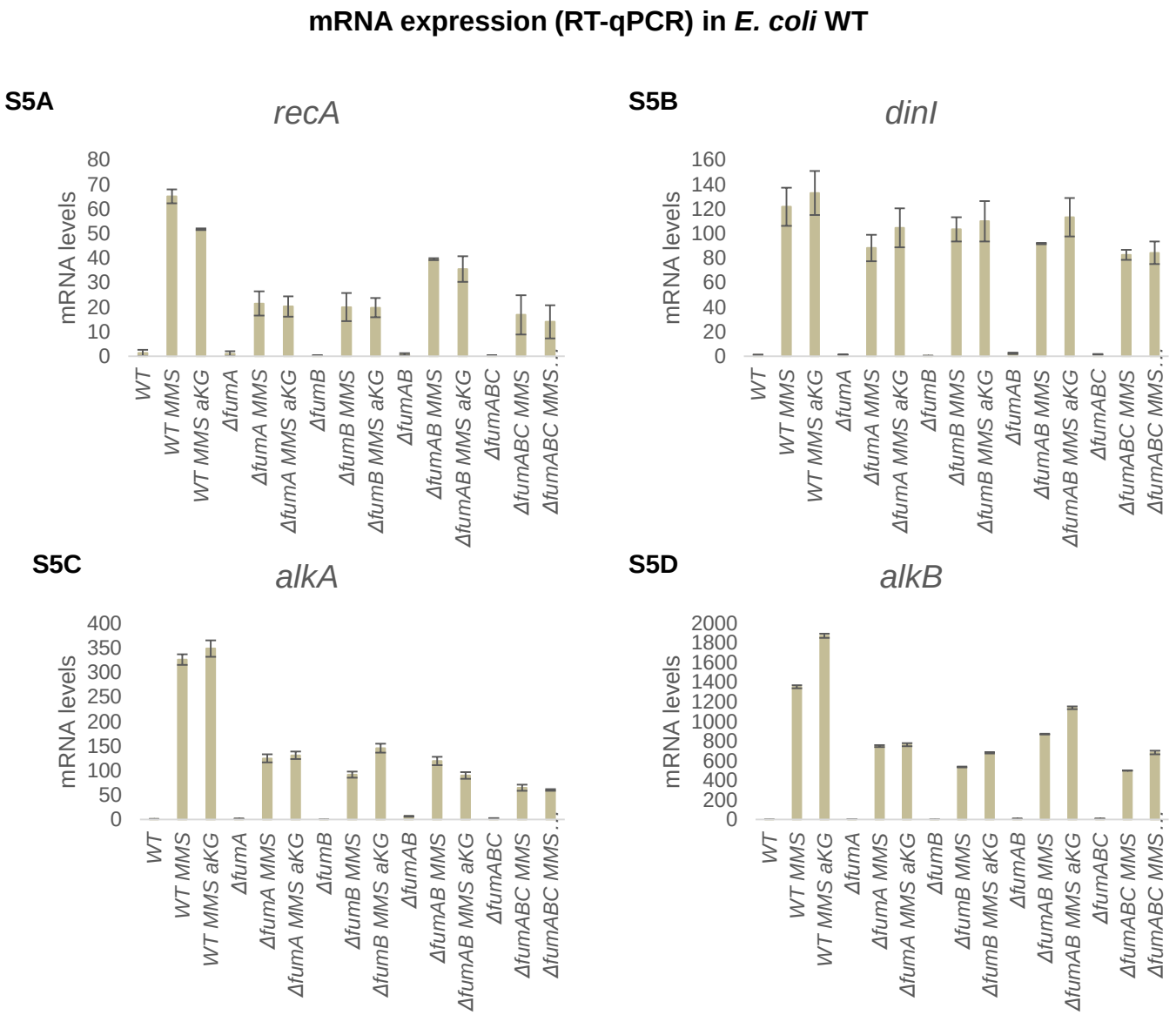

Figure S5- Validation of RNA-seq data. (**A-D**) *E. coli* wild type (WT), *ΔfumA, ΔfumB, ΔfumAB* and *ΔfumACB* strains were grown in LB and LB+25mM α-KG to early exponential phase (OD 600nm=0.3), treated with 0.35% [v/v] MMS for 45 minutes at 37°C. Cells were collected and total RNA was extracted. Graphs show mRNA expression levels of (**A**) *recA* (**B**) *dinI* (**C**) *alkA* and (**D**) *alkB* normalized against *gyrA* as an internal control and calculated using the ΔΔCT method. Data is represented as mean ± standard error (*n=3*).